

EXCURSION SET MASS FUNCTIONS FOR HIERARCHICAL GAUSSIAN FLUCTUATIONS

J. R. BOND,¹ S. COLE,² G. EFSTATHIOU,³ AND N. KAISER¹

Received 1990 July 23; accepted 1990 December 28

ABSTRACT

Most schemes for determining the mass function of virialized objects from the statistics of the initial density perturbation field suffer from the “cloud-in-cloud” problem of miscounting the number of low-mass clumps, many of which would have been subsumed into larger objects. We propose a solution based on the theory of the excursion sets of $F(\mathbf{r}, R_f)$, the four-dimensional initial density perturbation field smoothed with a continuous hierarchy of filters of radii R_f . We identify the mass fraction of matter in virialized objects with mass greater than M with the fraction of space in which the initial density contrast lies above a critical overdensity when smoothed on some filter of radius greater than or equal to $R_f(M)$. The differential mass function is then given by the rate of first upcrossings of the critical overdensity level as one decreases R_f at constant position \mathbf{r} . The shape of the mass function depends on the choice of filter function. The simplest case is “sharp k -space” filtering, in which the field performs a Brownian random walk as the resolution changes. The first upcrossing rate can be calculated analytically and results in a mass function identical to the formula of Press and Schechter—complete with their normalizing “fudge factor” of 2. For general filters (e.g., Gaussian or “top hat”) no analogous analytical result seems possible, though we derive useful analytical upper and lower bounds. For these cases, the mass function can be calculated by generating an ensemble of field trajectories numerically. We compare the results of these calculations with group catalogs found from N -body simulations. Compared to the sharp k -space result, less spatially extended filter functions give fewer large-mass and more small-mass objects. Over the limited mass range probed by the N -body simulations, these differences in the predicted abundances are less than a factor of 2 and span the values found in the simulations. Thus the mass functions for sharp k -space and more general filtering all fit the N -body results reasonably well. None of the filter functions is particularly successful in identifying the particles which form low-mass groups in the N -body simulations, illustrating the limitations of the excursion set approach. We have extended these calculations to compute the evolution of the mass function in regions that are constrained to lie within clusters or underdensities at the present epoch. These predictions agree well with N -body results, although the sharp k -space result is slightly preferred over the Gaussian or top hat results.

Subject headings: cosmology — galaxies: clustering — numerical methods

1. INTRODUCTION

In the context of hierarchical gravitational instability models, much effort has been focused on obtaining approximations to the mass function $n(M)dM$ of virialized objects directly from the statistics of the initial density field. The basic assumption here is that there is a reasonable correspondence between the sites of formation of virialized structures and regions which are above some threshold when filtered on a suitable scale. Within this basic framework, two similar formulations have been widely used to estimate $n(M)dM$, one based on *excursion sets*, i.e., regions where the density perturbation exceeds some threshold, using the classic Press-Schechter (1974, hereafter PS) formula (e.g., Schaeffer & Silk 1985, 1988; Kaiser 1988; Cole & Kaiser 1988, 1989; Efstathiou et al. 1988; Efstathiou & Rees 1988; Narayan & White 1987; Carlberg & Couchman 1988), and the other on the theory of *peaks* of the filtered Gaussian field (e.g., Bardeen et al. 1986; Bond 1987, 1988a, b; Bond, Szalay, & Silk 1988; Carlberg & Couchman 1988; Babul 1990). As emphasized by Bardeen et al. (1986, hereafter BBKS), none of these approaches are theoretically satisfactory since they fail to solve the cloud-in-cloud problem: in a hierarchical theory, clouds contain still smaller clouds, hence there is a danger of miscounting the number of objects.

Although the Press-Schechter (1974) formula has been used by many authors and has been found to agree well with mass functions from N -body experiments (Efstathiou et al. 1988), the derivation provided by Press & Schechter is far from convincing. In particular, by considering overdense regions in the initial linear density field, they derive an expression for the mass-function which accounts for only *half* of the mean mass density of the universe. They achieve the correct normalization by multiplying their expression by a factor of 2, though with little rigorous justification. As we show below, the Press-Schechter factor of 2 is closely connected with the cloud-in-cloud problem.

To solve the cloud-in-cloud requires (at least) some algorithm for excluding subclumps. Given a realization of a random initial perturbation field, one might well proceed as follows: First, filter the field with a very large radius and look for regions above the chosen threshold. Provided the filter radius is large enough, there will be no such regions. Now gradually decrease the filter radius until the highest density spot just touches the threshold and label the material within a filter radius of that spot as comprising an object of the appropriate mass. Next, reduce the filter radius until the next overdensity peak reaches the threshold and similarly tag

¹ CIAR Cosmology Program, Canadian Institute for Theoretical Astrophysics, McLennan Labs., University of Toronto, Toronto, ON, Canada M5S 1A1.

² Department of Astronomy and Center for Particle Astrophysics, University of California, Berkeley, Berkeley, CA 94720.

³ Department of Astrophysics, Oxford University, Oxford, UK OX1 3RH.

the material around that peak—but only if the material has not already been counted. In this way, one can construct a “group catalog” which explicitly avoids the cloud-in-cloud problem. Attempts along these lines were the “block” model of Cole & Kaiser (1988) and Cole (1991) and the hierarchical peaks model described in Bond (1989). The goal of this paper is to make more elaborate (and hopefully more realistic) predictions in the same vein. Rather than try to implement the scheme described above exactly, we solve a somewhat simpler, but closely related problem. Rather than follow peaks as a function of resolution scale and then tag material around the peaks, we simply follow field points and identify the cumulative mass fraction (i.e., the fraction of material in objects of mass $> M$) with the fraction of space in which the initial density contrast lies above a critical overdensity threshold when smoothed with any filter of radius greater than or equal to $R_f(M)$.

The “best” approach for deriving mass functions from initial conditions is a matter of debate and different possibilities give rise to different approximations to $n(M)dM$. However, these formulae can be objectively tested with N -body studies. Efstathiou et al. (1988) and Efstathiou & Rees (1988) demonstrated that the PS formula gives reasonable fits to the results derived from N -body simulations of power-law fluctuation spectra and the cold dark matter (CDM) model respectively. Carlberg & Couchman (1988) claim that while the PS formula describes the potential well distribution, the peak formalism provides a better fit to the galaxy distribution, as determined in their CDM “sticky particle” code.

In our approach, one is led to consider the statistics of the four-dimensional field $F(\mathbf{r}, R_f)$, and, in particular, the “trajectories” of the field as a function of filter radius at fixed position. The differential mass function, for instance, is then simply expressible in terms of the rate at which these random trajectories meet an absorbing barrier. In § 2, we discuss the topology of the $F(\mathbf{r}, R_f)$ field for various choices of filter, illustrating the results with realizations of random fields in one spatial dimension. We find very different structural behavior for Gaussian filtering, for top hat filtering and for sharp k -space filtering. In § 3 we solve the absorbing barrier problem for three-dimensional fields. The simplest case is that of sharp k -space filtering, for which we obtain an exact analytical result. This result turns out to be identical to the approximation of Press & Schechter, complete with their “fudge” factor of 2 discussed above! We show how this result may be derived either from a diffusion equation (Fokker-Planck approach) or by solving a simple Langevin equation for the field amplitude F . One might well imagine that other choices of filter would give better results. Unfortunately, for such filters the calculation is more difficult. While the trajectories are still random walks of a kind, there are nontrivial correlations, and, consequently, no analog of the sharp k -space diffusion equation applies. We have been able to obtain analytic upper and lower bounds on the mass function but have been forced to resort to making realizations and following Langevin trajectories numerically to obtain the mass function. Fewer high-mass rare events and more small-mass objects are predicted for both Gaussian and top hat filtering compared to sharp k -space. Peacock & Heavens (1990) have also demonstrated this using one-dimensional reconstructions of the density field. In § 4 we compare the resulting mass functions with those obtained from N -body simulations. In § 5 we generalize our approach to obtain the mass function at some early time for regions which today are in rich clusters or other special regions. In this way, we can quantify how the dark matter condensations are biased. Again, we compare the results with N -body simulations and find good agreement. In § 6, we discuss strengths and limitations of the overall approach, especially in regard to the determination of the abundances of rare events. We emphasize that although we have formally solved the cloud-in-cloud problem in the excursion set approach, the utility of the solution depends upon the way we relate the linear overdensity F and filter scale R_f characterizing the linear Gaussian perturbations to the final properties of the virialized entities, e.g., using spherical “top hat” models to map (F, R_f) to the final virialized values (δ_v, M) .

2. THE TOPOLOGY OF GAUSSIAN FIELDS IN POSITION AND RESOLUTION SPACE

We start with a density perturbation field $F(\mathbf{r})$ which is a homogeneous and isotropic Gaussian random field uniquely specified by its power spectrum. The hierarchical fields that we shall consider (such as the CDM model) have structure on all scales, so we are led immediately to consider the $(N + 1)$ -dimensional field $F(\mathbf{r}, R_f)$ smoothed by convolving with a smoothing function $W(\mathbf{r}; R_f)$ on resolution scale R_f :

$$F(\mathbf{r}, R_f) = \int d^3 r' W(\mathbf{r} - \mathbf{r}') F(\mathbf{r}', 0), \quad F(\mathbf{k}, R_f) = \tilde{W}(kR_f) F(\mathbf{k}, 0). \quad (2.1)$$

Here $\tilde{W}(kR_f)$ is the Fourier transform of W . Of course, the homogeneity and isotropy is not preserved in the resolution direction. Assuming linear theory, the field $F(\mathbf{r}, R_f)$ grows in amplitude in proportion to $D(t)$, where $D(t)$ is the linear growth factor (Peebles 1980, § 2.11). Here, instead of viewing the field $F(\mathbf{r}, R_f)$ to be growing in amplitude relative to a fixed threshold f_v , we consider $F(\mathbf{r}, R_f)$ to be of fixed amplitude and use a threshold that decreases with time. Thus we take $F(\mathbf{r}, R_f)$ to be the initial linear density field extrapolated to the present time t_0 using linear theory and use a threshold that decreases with t as $f_v/D(t)$, with $D(t_0) = 1$. [For $\Omega = 1$ universes dominated by nonrelativistic matter, $D(t) = (1 + z)^{-1}$, in terms of the redshift z .]

To help visualize the complex topology defined by the $F(\mathbf{r}, R_f)$ surface, let us consider the $N = 1$ case. The two-dimensional surface $F(\mathbf{r}, R_f)$ defined by a realization of a one-dimensional Gaussian random field is shown in Figure 1 for two different choices of filter function. Figures 2 and 3 then show the intersection of this surface with a threshold f_v , and selected trajectories of $F(\mathbf{r}, R_f)$ with R_f , respectively. Figure 1 brings to mind a topographic map. If we take slices through this at constant R_f , then for large R_f we have smooth rolling hills and valleys oriented roughly parallel to the R_f axis, of relatively small elevations and depressions. As we proceed to smaller R_f these give way to mountains and trenches of greater amplitude and smaller coherence length. On the other hand, if we take a slice at constant position r we obtain some kind of random walk with the field fluctuating to larger and larger values with decreasing resolution length. Extrema of $F(r)$ correspond to ridge lines and riverbeds of the $F(\mathbf{r}, R_f)$ surface.

The underlying assumption in this study is that the gravitationally bound structures forming at any epoch t are to be identified with regions above some critical initial overdensity $F = f_v/D(t)$; for a given time (the present, say) this would be a plane of constant elevation. Were we to submerge this landscape to the level $f_v/D(t)$, we would have an ocean extending from $R_f = \infty$ to some

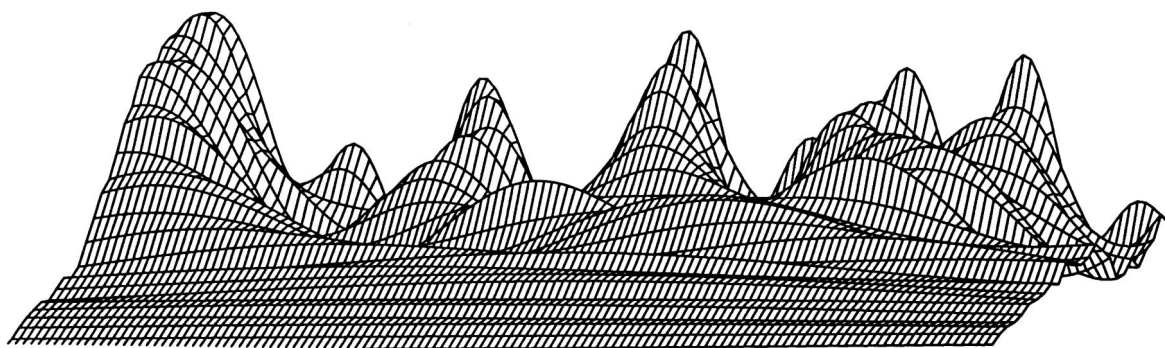


FIG. 1a

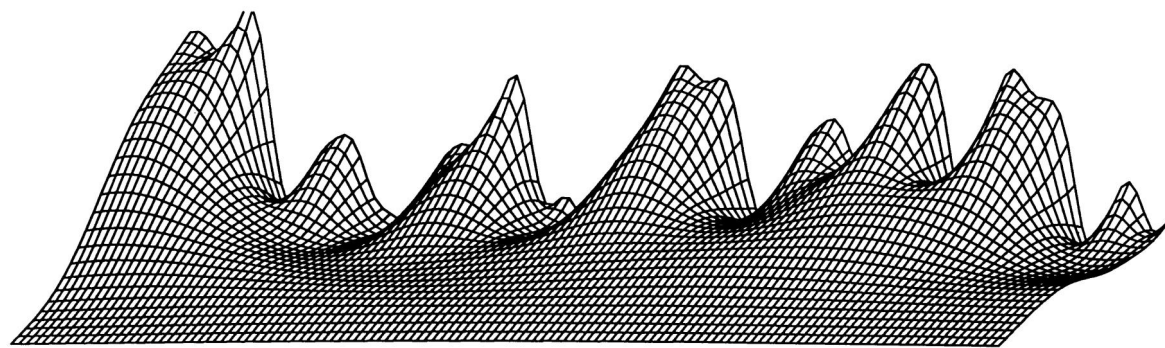


FIG. 1b

FIG. 1.—Topographical maps of one-dimensional Gaussian random density fields $F(r, \Lambda)$ as a function of position and resolution for (a) sharp k -space filtering and (b) Gaussian filtering. The spectra are $n = 0$ power laws. The depth dimension is $\log_{10}(R_f)$, with a spacing of 0.06 and depth coverage a factor of 1.5. The horizontal dimension is position r , the range is 1/64 of the box the field was generated on. The range in the rms amplitude is $(32)^{1/2}$.

shoreline $R_f(r)$ —the first upcrossing contour. While we would also find inland bodies of water, and these might contain islands or peninsulas, these are clearly distinct from the ocean.

We define a variable $\Lambda \equiv \sigma_F^2$ which in this paper will be called the “resolution” and which acts like a pseudo-time variable:

$$\Lambda \equiv \sigma_F^2(R_f) \equiv \int \frac{d^3k}{(2\pi)^3} \langle |F(k, R_f)|^2 \rangle. \quad (2.2)$$

Λ is just the variance of the density field at resolution R_f . In this paper, we consider the following three filters:

(1) Sharp k -space:

$$W_K(r; R_k) = (4\pi R_k^3/3)^{-1} 3(\sin x - x \cos x)/x^3, \quad x \equiv r/R_k, \\ \tilde{W}_K(k; R_k) = 9(1 - kR_k); \quad (2.3a)$$

(2) Gaussian:

$$W_G(r; R_f) = \exp(-r^2/2R_f^2)(2\pi R_f^2)^{-3/2}, \\ \tilde{W}_G(k; R_f) = \exp(-R_f^2 k^2/2); \quad (2.3b)$$

(3) Top Hat:

$$W_{TH}(r; R_{TH}) = 9 \left(1 - \frac{r}{R_{TH}}\right) \left(\frac{4\pi}{3} R_{TH}^3\right)^{-1}, \\ \tilde{W}_{TH}(k; R_{TH}) = 3(\sin x - x \cos x)/x^3, \quad x \equiv kR_{TH}. \quad (2.3c)$$

The choice of sharp k -space or Gaussian filtering is primarily motivated by convenience of analysis. These filters have the disadvantage that it is not easy to associate a well-defined mass with R_f (beyond the simple dimensional consideration that M should scale as R_f^3). This is a serious disadvantage since the goal is to predict $n(M)dM$, i.e., the number density of objects in the mass range M to $M + dM$. The problem can only be solved by calibration against N -body computations. The top hat filter partially



FIG. 2a

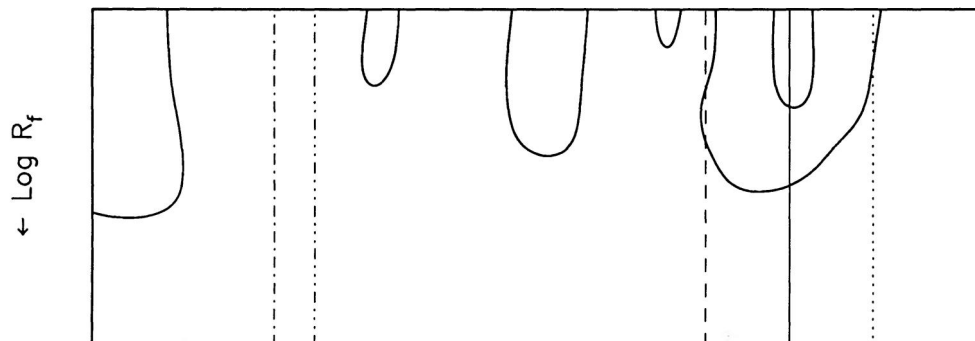


FIG. 2b

FIG. 2.—Plots of a single contour surface $F = f_v$ for the same field configurations as in Fig. 1, except that the spacing is 0.03 in $\log_{10}(R_f)$, for (a) sharp k -space and (b) Gaussian filtering. Smaller values do not affect the contours in (b), but those in (a) become jagged on arbitrarily fine scales. For one-dimensional fields the mass M is proportional to R_f . At the five positions indicated, the intercepts with the contour are successively up then down crossings. In (b) the one nested contour has the first extremal corresponding to a peak (necessarily upcrossing) and the second a minimum (necessarily downcrossing). This is evident from the relevant section of the surface plot Fig. 1.

avoids this problem—the mass is reasonably well defined. However, for density fields like that of the cold dark matter (CDM) model, this filter produces a smoothed density field which is not differentiable with respect to position r (if scale-invariance holds on all scales).

The example shown in Figure 1b was calculated with a Gaussian filter. This gives a smooth continuously varying surface with ridges and valleys which are also continuous (with the exception of points where, for instance, a ridge line bifurcates to two ridges straddling a valley). This continuity is not shared by the top hat filter case. A special feature of Gaussian filtering is that all ridges increase in elevation with decreasing R_f and conversely for valleys. This means that with this filtering there can be no “lakes” of finite extent, and the ocean shoreline can have no bays—there may be promontories, but the shoreline can never reverse its curvature to connect these; between any pair of promontories there must be at least one ocean inlet extending to arbitrarily small R_f . Another property of Gaussian filtering is that the variance is a monotonically decreasing function of R_f . For other filters this may not be strictly true, but for the power spectra of interest here this is probably a generic feature.

The sharp k -space filter gives rise to a surface with some very interesting properties, as illustrated by Figure 1a. With this filter, the transition from one filter radius to a smaller one is obtained by adding a statistically independent random field. This has the perhaps unsettling consequence that the $F(r, R_f)$ surface will no longer be differentiable with respect to R_f , so one must speak cautiously about peaks or ridge lines. Slices at constant r are in this case precisely Brownian random walks.

Applying this topological language to the derivation of the Press-Schechter formula, the cumulative mass fraction [which we denote by $\Omega_v(M)/\Omega$ where Ω is the density of the universe in units of the closure density and the mass M is a function of R_f] is identified with the fraction of dry land. This is perhaps not unreasonable for large filter radii where $\Omega_v(M)/\Omega \ll 1$. On the high mass end of the distribution, most objects of mass $> M$ are actually very close to M , so if we reduce the filter radius by a factor of 2 say, we will generate a set of new excursion regions. These, for the most part, will have a size similar to the filter radius, so it seems reasonable to associate the change in total volume of excursion regions with the net mass in objects of this scale. The problem is that at small filter radii even regions which lay above the threshold for some larger filter will break up into roughly equal areas above

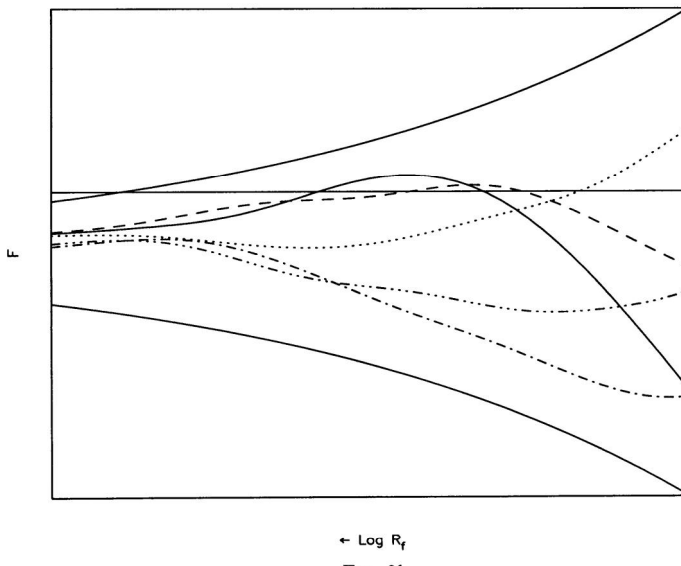
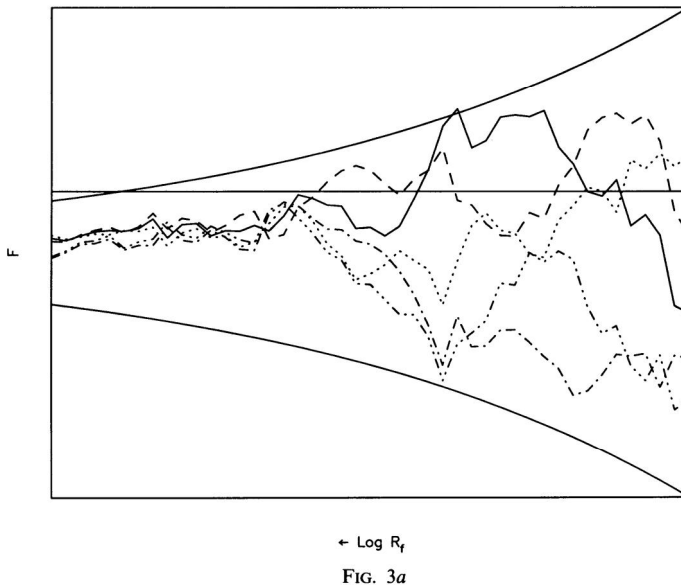


FIG. 3.—The trajectories as functions of filter radius R_f at the five r -positions marked by vertical lines in Fig. 2 in the corresponding line style. The threshold line $F = f_v$ and the 2σ envelope are also shown. The trajectories in (a) are true Brownian random walks with a discrete step size which is determined by the spacing in R_f of the filters used. The corresponding trajectories in (b) are smooth curves and exhibit long-range correlations.

and below the threshold, and it is not easy to see why one should associate the resulting variation in the fraction of dry land as a function of resolution with the mass in clumps at that scale.

The cumulative mass fraction we propose is identified with the most southerly⁴ shore (f_v -contour) of the ocean along due north paths. This excludes bays unless they are pointing due south as well as inland waterways. The differential mass function is proportional to the rate at which trajectories (lines of constant r), such as those shown in Figure 3, first upcross the shore. In the language of Peacock & Heavens (1990) this corresponds to the decay of the survival probability. The differential mass function is obtained from this by dividing by the mass $M(R_f)$ associated with the filtering scale R_f :

$$n(M)dM = \frac{\bar{\rho}_0}{M} \frac{1}{\Omega} \frac{d\Omega_v(M)}{dM} dM , \quad (2.4)$$

where $\bar{\rho}_0$ is the average cosmological density.

⁴ We have defined the direction of decreasing R_f as north.

3. THE ABSORBING BARRIER PROBLEM

3.1. Sharp k -Space Filtering

In the case of sharp k -space filtering, when one increases the resolution from Λ to $\Lambda + \Delta\Lambda$, the increment to $F(\mathbf{r}, \Lambda)$ is composed of the extra high- k modes accepted by the filter. For a Gaussian random field the phases of these new high- k modes are random and uncorrelated with those of lower k . Thus the increment to $F(\mathbf{r}, \Lambda)$ is a statistically independent Gaussian random field with zero mean and variance $\sigma_\Delta^2 = \Delta\Lambda$, and the trajectories follow precisely Brownian random walks. The rate of first upcrossings at a threshold (or the rate of absorption of particles onto an absorbing barrier) was calculated by Chandrasekhar (1943). He gave a simple graphical solution which we translate into the language of our problem and reproduce here.

If we think of our field trajectories as particles randomly walking in field space, the problem we wish to solve can be posed as follows: given a source of particles at $F = 0$, find $\Omega_v(M)/\Omega$, the fraction of particles which will have been absorbed on a barrier at $F = f_v$ by "time" Λ . In the absence of a barrier, the distribution of particle positions is just the Gaussian

$$P(F)dF = \frac{dF}{\sqrt{2\pi\Lambda}} \exp\left(-\frac{F^2}{2\Lambda}\right).$$

To obtain $\Omega_v(M)$, we need to integrate over this barrier-free distribution, but only counting trajectories which have crossed the $F = f_v$ line. Now above the threshold, all trajectories have passed the threshold, so this contributes the area under the tail of the Gaussian to $\Omega_v(M)/\Omega$. Chandrasekhar noted that for each trajectory which reaches a field value above the threshold, there is an equally likely trajectory obtained by reflecting about the threshold the portion of the trajectory beyond the point where it first pierces the threshold f_v (see Fig. 4). Thus, one obtains the distribution

$$\Pi(F, \Lambda, f_v) = \frac{1}{\sqrt{2\pi\Lambda}} \left\{ \exp\left[-\frac{F^2}{2\Lambda}\right] - \exp\left[-\frac{(2f_v - F)^2}{2\Lambda}\right] \right\}, \quad (3.1)$$

for paths which have not met the threshold, and the cumulative mass fraction is just twice the area in the tail of the Gaussian.

A more formal path to this solution is via a diffusion equation. The distribution function Π satisfies a Smoluchowski (Chapman-Kolmogorov) equation

$$\Pi(F_n, \Lambda_n, f_v) = \int_{-\infty}^{\infty} dF_{n-1} P(F_n, \Lambda_n | F_{n-1}, \Lambda_{n-1}) \Pi(F_{n-1}, \Lambda_{n-1}, f_v), \quad (3.2)$$

which states that the distribution at resolution Λ_n only depends upon the distribution at the immediately prior resolution, possibly infinitesimally earlier. The connection between the two times occurs through a transition probability $P(F_n, \Lambda_n | F_{n-1}, \Lambda_{n-1})$, whose form is easily obtained, since it is the ordinary conditional probability giving field values at Λ_n given the values at Λ_{n-1} . It is the

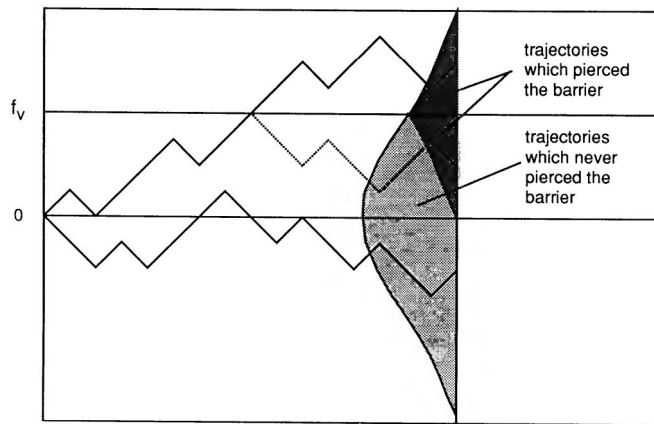


FIG. 4.—This figure shows schematically examples of random walks of $F(\mathbf{r}, \Lambda)$ with Λ . In the limit of infinitesimally fine steps in Λ the distribution of trajectories at fixed Λ is Gaussian as indicated by the curve on the right of the figure. The heavily shaded fraction of this Gaussian above the barrier at $F = f_v$ represents the fraction of trajectories above the barrier at Λ . For such a trajectory, if one reflects in the barrier the portion that lies to the right of where it first pierces the barrier, one obtains, for example, the dotted trajectory. This new trajectory is just as likely as the one it was formed from. Consequently the heavily shaded region below the barrier, which is simply the reflection of the region above the barrier, represents the probability of a trajectory being below the barrier at Λ but having pierced the barrier at some lower value of Λ . Thus the lightly shaded fraction of the area under the Gaussian represents the fraction of trajectories which have not pierced the barrier at any lower value of Λ .

Gaussian

$$P(F + \Delta F, \Lambda + \Delta \Lambda | F, \Lambda) = \frac{1}{\sqrt{2\pi}\sigma_\Delta} \exp\left[-\frac{-(\Delta F - \bar{\Delta F})^2}{2\sigma_\Delta^2}\right], \quad (3.3a)$$

$$\bar{\Delta F} = \langle \Delta F | F \rangle = \frac{\langle F \Delta F \rangle}{\langle F^2 \rangle} F, \quad (3.3b)$$

$$\sigma_\Delta^2 = \langle (\Delta F - \bar{\Delta F})^2 | F \rangle = \langle (\Delta F)^2 \rangle - \frac{\langle F \Delta F \rangle^2}{\langle F^2 \rangle}, \quad (3.3c)$$

expressed in terms of the variables $F = F_{n-1}$, $\Delta F \equiv F_n - F_{n-1}$, $\Lambda = \Lambda_{n-1}$ and $\Delta \Lambda \equiv \Lambda_n - \Lambda_{n-1}$. A Fokker-Planck equation follows from equation (3.3) by expanding in powers of ΔF and letting $\Delta \Lambda$ go to zero:

$$\frac{\partial \Pi}{\partial \Lambda} = \lim_{\Delta \Lambda \rightarrow 0} \frac{1}{\Delta \Lambda} \left[\frac{1}{2} \frac{\partial^2 \langle (\Delta F)^2 | F \rangle \Pi}{\partial F^2} - \frac{\partial \langle \Delta F | F \rangle \Pi}{\partial F} \right]. \quad (3.4)$$

For sharp k -space filtering, $\langle F \Delta F \rangle = 0$, $\langle (\Delta F)^2 \rangle = \Delta \Lambda$, so the drift term vanishes and we are left with the simple diffusion equation

$$\frac{\partial \Pi}{\partial \Lambda} = \frac{1}{2} \frac{\partial^2 \Pi}{\partial F^2}. \quad (3.5)$$

To solve this we need to supply in addition the boundary condition that $\Pi = 0$ at $F = f_v$. It is easy to verify that equation (3.1) does satisfy equation (3.5) with this boundary condition.

Since $F(\mathbf{r}, \Lambda)$ describes a random walk, the theoretical apparatus of Brownian motion can also be applied to this problem. The trajectory of the field $F(\mathbf{r}, \Lambda)$ as a function of Λ at a fixed point \mathbf{r} obeys a Langevin evolutionary equation:

$$\frac{\partial F}{\partial \ln k} (\mathbf{r}, \ln k) = Q_F(\mathbf{r}, \ln k). \quad (3.6a)$$

Instead of using Λ as an integration variable, it is more convenient to use $\ln k$, where k is the sharp k -space filter. In equation (3.6a), Q_F is a Gaussian-distributed stochastic force, a Markov random variable with zero mean and dispersion

$$\langle Q_F(\mathbf{r}_1, \ln k_1) Q_F(\mathbf{r}_2, \ln k_2) \rangle = \delta(\ln k_1 - \ln k_2) \mathcal{P}_\rho(k_1) \frac{\sin k_1 r}{k_1 r}, \quad r = |\mathbf{r}_1 - \mathbf{r}_2|, \quad (3.6b)$$

where

$$\mathcal{P}_\rho(k) \equiv \frac{d\Lambda(k)}{d \ln k} = \frac{k^3 \langle |F_k|^2 \rangle}{(2\pi^2)} \quad (3.6c)$$

is the (linear) power spectrum evaluated at the current epoch. The Markov nature of the trajectories is embodied in the delta function in $\ln k$, expressing the lack of correlation between one stochastic impulse and the next.

A straightforward method for obtaining the virialized fraction is to evaluate the frequency with which trajectories calculated using the Langevin equation first pierce the $F = f_v$ absorbing barrier, starting from $F = 0$ at $\Lambda = 0$. Although this exercise just confirms the analytic result obtained below, it also demonstrates a viable numerical method for obtaining the collapsed fraction for other filters where it is not possible to derive analytic solutions. The agreement is shown in Figure 5a for a cold dark matter model fluctuation spectrum, obtained with 4200 wavenumbers spaced equally in $\ln k$. Similar agreement can be obtained with as few as 1000 wavenumbers.

We equate the fraction of mass in objects with mass greater than M , $\Omega^{-1} \Omega_v(M)$, to the fraction of trajectories which are absorbed by the barrier at f_v at resolution less than $\Lambda(M)$. Hence in our notation

$$\frac{\Omega_v(M)}{\Omega} = 1 - \int_{-\infty}^{f_v} dF \Pi(F, \Lambda, f_v), \quad (3.7)$$

where the distribution of trajectories which have remained below the barrier, $\Pi(F, \Lambda, f_v)$, is given by equation (3.1). This yields the differential mass fraction

$$\frac{1}{\Omega} \frac{d\Omega_v(M)}{d \ln M} = - \left(\frac{d \ln \Lambda}{d \ln M} \right) \left[\frac{d}{d \ln M} \int_{-\infty}^{f_v} dF \Pi(F, \Lambda, f_v) \right], \quad (3.8)$$

which, using the diffusion equation (3.5), readily simplifies to

$$\frac{1}{\Omega} \frac{d\Omega_v(M)}{d \ln M} = \frac{d \ln \Lambda}{d \ln M} \left(\frac{-\Lambda}{2} \right) \left[\frac{\partial \Pi(F, \Lambda, f_v)}{\partial F} \right]_{F=-\infty}^{F=f_v} = - \frac{1}{\sqrt{2\pi}} \frac{f_v^2}{\Lambda^{1/2}} \exp\left(-\frac{f_v}{2\Lambda}\right) \frac{d \ln \Lambda}{d \ln M}. \quad (3.9)$$

This expression is identical to the Press-Schechter formula *including* the ad hoc multiplicative factor of 2 that Press & Schechter

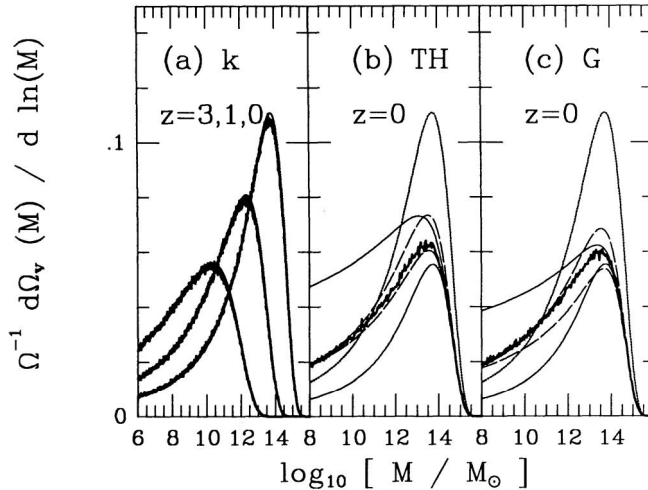


FIG. 5.—In (a), the sharp k -space (Press-Schechter) result for the $b_\rho = 1.7$, $h = 0.5$ CDM model is compared with the distribution function computed using 2×10^6 Langevin trajectories for the redshifts shown. In (b) and (c), the top hat and Gaussian computations with 10^6 trajectories (heavy solid curves) are compared with the sharp k -space result (dotted), the up and up-down analytic results of § 3.3.1 (solid), the Peacock-Heavens approximation (upper dashed curve) and the no-correlation approximation (lower dashed curve). 4200 wavenumbers were used between 5×10^{-3} and 10^3 Mpc $^{-1}$ for (a), 2200 for (b) and (c).

introduced to satisfy the constraint $\int d\Omega_v(M)/\Omega = 1$. In fact, it is easy to see where the factor of 2 comes from in our derivation and why it was missed by Press and Schechter, for it corresponds to the mass density in collapsed structures contributed by the second term on the right-hand side of equation (3.1). Physically, this corresponds to mass elements that lie below the threshold f_v at resolution $\Lambda(M)$ but exceed the threshold at a lower resolution and are therefore assigned to collapsed objects more massive than M . Press & Schechter ignore such trajectories and assert that the fraction of mass in objects of mass $\geq M$ is given by the fraction of mass above f_v at resolution $\Lambda(M)$ —which is clearly false, as our derivation shows.

3.2. General Filters

3.2.1. Monte Carlo Simulations

For a nonsharp k -space filter, the problem is considerably more complicated. One can no longer express the distribution at one time as a simple convolution of the distribution at a slightly earlier time with a fixed transition probability; i.e., the process is non-Markov. Instead, the probability,

$$\Pi(F_n, \Lambda_n, f_v) dF_n \equiv dF_n \int_{-\infty}^{f_v} dF_{n-1} \dots \int_{-\infty}^{f_v} dF_1 P(f_n, \Lambda_n; F_1, \Lambda_1; F_2, \Delta_2; \dots; F_{n-1}, \Lambda_{n-1}), \quad (3.10)$$

that the field lies below f_v for steps 1 to $n-1$ and has value in the interval F_n to $F_n + dF_n$ on step n depends on the entire history. The non-Markovian nature of the variable F implies that no analog of the Smoluchowski equation (3.2) for $\Pi(F, \Lambda, f_v)$ exists.⁵

We can, however, determine the required distributions by a Monte Carlo approach. We require a large number of trajectories $F(r, R_f)$ as a function of filtering radius R_f . To construct these, we integrate a series of Langevin equations over wavenumber k :

$$\frac{\partial F}{\partial \ln k}(r, R_f, \ln k) = Q_F(r, \ln k) \tilde{W}(kR_f), \quad \langle Q_F(r_1, \ln k_1) Q_F(r_2, \ln k_2) \rangle = \delta(\ln k_2 - \ln k_1) \mathcal{P}_\rho(k_1) \frac{\sin k_1 r}{k_1 r}. \quad (3.11)$$

The stochastic forces Q_F are identical to those of equation (3.6). We build up the entire trajectory on a grid in resolution space by successively adding the stochastic forces as we sweep through $\ln k$ space. The spacing in R_f is chosen to satisfy two criteria: that the fractional change in F is small in any step and that the absolute change is small compared with whatever threshold levels f_v are of interest. The former suggests equal spacing in $\ln \Lambda^{1/2}$, and the latter equal spacing in $\Lambda^{1/2}/f_v$. To approximate this, we step in equal intervals in $\ln R_f$ for large R_f , then in equal steps in $R_f^{-p_s}$, where p_s is a power designed to make the steps approximately equal in $\Lambda^{1/2}$. For the power law fluctuation spectra of index n [with $\mathcal{P}_\rho(k) \propto k^{3+n}$] that we treat in § 4, we would choose $p_s = (n+3)/2$. The boundary between the two sampling procedures is determined when the step size with log sampling first exceeds the step size with power law sampling. For the calculations shown in Figure 5, about 280 radii were chosen for (b) and (c), respectively. Larger numbers are not required since the trajectories are relatively coherent, as we show below. There are a number of methods we have

⁵ One must be careful not to confuse $\Pi(F, \Lambda, f_v)$ with the one-point probability $P(F, \Lambda) dF$ that the field lies between F and $F + dF$ at resolution Λ , irrespective of prior value. For all filters $P(F, \Lambda) dF$ does obey a Smoluchowski equation and the associated “Fokker-Planck” equation has a drift term only, with no diffusion term. Thus only one condition on P can be specified, an initial condition at $\Lambda = 0$. The general solution is a function only of $F/\sqrt{\Lambda}$, which leads to the usual Gaussian $P(F, \Lambda) = e^{-F^2/2\Lambda}/(2\pi)^{1/2}$. The final condition at $F = f_v$ that was necessary to get eq. (3.1) cannot be imposed.

adopted to speed up the computations. Large steps in R_f can be taken if a path is well away from the barriers of interest, with small steps required only near the barrier. As well, the trajectories only have to be computed until the first upcrossing through the highest barrier. Although 2200 steps equally spaced in $\ln k$ were used for Figures 5b and 5c, we have found it feasible to perform calculations with an order of magnitude more wavenumbers. Top hat filtering requires more computational effort than Gaussian filtering, especially for steeper spectra. We found it useful to slightly round the corners of the top hat with a weak Gaussian smoothing with Gaussian filtering radius one-tenth the top hat radius. This is especially important for steep spectra (for index $n \geq 1$, Λ would not even converge otherwise).

Another numerical approach, adopted by Peacock & Heavens (1990) and checked by us, uses a one-dimensional FFT. One can easily and often, for a suite of filtering radii, do 64000 spatial points, thereby generating an ensemble of trajectories. Although there are more wavenumbers with an FFT, they are not optimally spaced for accuracy over a wide range and one cannot practically do as many filtering radius as one can with our approach.

The results of our Langevin calculations for various scale free universes are given in Figure 9 of § 4, where we make comparisons with the results of N -body simulations. Calculations for a cold dark matter spectrum are given in Figures 5a and 5b and are compared with various analytic approximations which we now describe.

3.2.2. Upcrossing and Downcrossing Points on the Absorbing Barrier

The calculation of the first upcrossing rate is made difficult because of the nonlocal condition that the history of the trajectory should lie below the threshold. We can obtain useful bounds on, and approximations to, the fraction of trajectories which have yet to upcross the barrier using the rate of up- and downcrossings calculated without regard to the previous history. It is useful to introduce various integer quantities: We denote the number of times the trajectory has upcrossed through f_v by resolution Λ by $N_{\text{up}}(\Lambda, f_v)$ and the number of times the trajectory has downcrossed through f_v by $N_{\text{down}}(\Lambda, f_v)$. They both increase in integer steps, while the difference, $N_{\text{ud}}(\Lambda, f_v) \equiv N_{\text{up}} - N_{\text{down}}$ is always zero or one. The length of time (i.e., resolution) after upcrossing that N_{ud} remains unity before a down “annihilates” the up is a measure of the coherence of the filter. The advantage of these three quantities is that their statistical averages are analytically tractable.

What we are interested in, of course, is the operator $N_{1\text{up}}(\Lambda, f_v)$, which is zero until the first upcrossing occurs, at which point it becomes unity. It has not proved possible to derive an expression for it in the general case. However, since, for each trajectory, we must have $N_{\text{up}}(\Lambda) \geq N_{1\text{up}}(\Lambda) \geq N_{\text{ud}}(\Lambda)$, the averages over an ensemble of paths must obey this as well, providing us with strict upper and lower bounds. We also always have $N_{\text{up}}(\Lambda) - N_{\text{up}}(\Lambda - \delta\Lambda) \geq N_{1\text{up}}(\Lambda) - N_{1\text{up}}(\Lambda - \delta\Lambda)$; hence $d\langle N_{\text{up}} \rangle / d\Lambda$ is also a strict upper bound for $d\langle N_{1\text{up}} \rangle / d\Lambda$. We compare the numerical results for $d\langle N_{1\text{up}} \rangle / d\Lambda$ with analytical calculations for $d\langle N_{\text{up}} \rangle / d\Lambda$ and $d\langle N_{\text{ud}} \rangle / d\Lambda$ for a biased CDM model in Figure 5.

It is useful to introduce statistical rate operators, defined as derivatives of these integer operators:

$$R_{\text{up}} \equiv \frac{dN_{\text{up}}}{d\Lambda} = \sum_{\Lambda_{\text{up}}} \delta(\Lambda - \Lambda_{\text{up}}) = |\dot{F}| \theta(\dot{F}) \delta(F - f_v), \quad (3.12a)$$

$$R_{\text{down}} \equiv \frac{dN_{\text{down}}}{d\Lambda} = \sum_{\Lambda_{\text{down}}} \delta(\Lambda - \Lambda_{\text{down}}) = |\dot{F}| \theta(-\dot{F}) \delta(F - f_v), \quad (3.12b)$$

$$R_{\text{ud}} \equiv R_{\text{up}} - R_{\text{down}} = \dot{F} \delta(F - f_v), \quad (3.12c)$$

where Λ_{up} denotes all those resolutions at which $F = f_v$ with $dF/d\Lambda > 0$, and Λ_{down} denotes the downcrossing resolutions ($dF/d\Lambda < 0$). Here the θ -function is the unit Heaviside step function. Although the expression as the sum of delta functions makes the meaning of these operators as point processes transparent, the form in terms of $\dot{F} \equiv dF/d\Lambda$ and F is obviously more useful for calculations.

We can also define a point process for the first upcrossing points:

$$R_{1\text{up}}(\Lambda, f_v) \equiv \frac{dN_{1\text{up}}}{d\Lambda} = \delta(\Lambda - \Lambda_{1\text{up}}) = R_{\text{up}}(\Lambda, f_v) \{1 - \theta[N_{\text{down}}(r, \Lambda)]\}. \quad (3.13)$$

The operator expression in terms of R_{up} and N_{down} is deceptively simple, but a closed form expression cannot be given for general filters as we describe in § 3.2.3.

We can easily evaluate the average of equations (3.12) using the joint Gaussian probability distribution $P(\dot{F}, F)$, which is very similar in form to that given in equation (3.3):

$$\langle R_{\text{up}} \rangle = \frac{e^{-v_v^2/2}}{\sqrt{2\pi}} \left[\frac{v_v}{\Lambda_\mu} + \frac{1}{\Lambda_c} \left\{ \frac{\exp[-\frac{1}{2}(\lambda v_v)^2]}{\sqrt{2\pi}} - \frac{1}{2} \lambda v_v \operatorname{erfc}\left(\frac{\lambda v_v}{\sqrt{2}}\right) \right\} \right], \quad (3.14a)$$

$$\langle R_{\text{down}} \rangle = \frac{e^{-v_v^2/2}}{\sqrt{2\pi}} \left[\frac{1}{\Lambda_c} \left\{ \frac{\exp[-\frac{1}{2}(\lambda v_v)^2]}{\sqrt{2\pi}} - \frac{1}{2} \lambda v_v \operatorname{erfc}\left(\frac{\lambda v_v}{\sqrt{2}}\right) \right\} \right], \quad (3.14b)$$

$$\langle R_{\text{ud}} \rangle = \frac{e^{-v_v^2/2}}{\sqrt{2\pi}} \frac{v_v}{\Lambda_\mu}, \quad (3.14c)$$

$$v_v \equiv \frac{f_v}{\Lambda^{1/2}}, \quad \lambda \equiv \frac{\Lambda_c}{\Lambda_\mu}.$$

Here, the two resolutions Λ_μ and Λ_c are related to the constrained average and dispersions of \dot{F} for fixed $F = f_v$:

$$\Lambda_\mu^{-1} \equiv -\frac{\langle \dot{F} | F \rangle}{F} = -\frac{\langle F \dot{F} \rangle}{\langle F^2 \rangle}, \quad (3.15a)$$

$$\Lambda_c^{-2} \equiv \frac{\langle (\Delta \dot{F})^2 | F \rangle}{\langle F^2 \rangle} = \frac{\langle \dot{F}^2 \rangle}{\langle F^2 \rangle} - \frac{\langle F \dot{F} \rangle^2}{\langle F^2 \rangle^2}, \quad (3.15b)$$

$$\Delta \dot{F} \equiv \dot{F} + \Lambda_\mu^{-1} F.$$

Note the similarity to the average and dispersion appearing in equation (3.3). We are to take the meaning of \dot{F} in equations (3.12) and (3.15) as a one-sided derivative, $[F(\Lambda) - F(\Lambda - \delta\Lambda)]/\delta\Lambda$ as $\delta\Lambda$ goes to zero. Only for sharp k -space filtering does this one-sidedness of the derivative make a difference.

Both Λ_μ and Λ_c are coherence scales of a sort. For resolution $\delta\Lambda = \Lambda_1 - \Lambda_2 > 0$, the two point function of the field in the resolution direction is

$$\langle F(\Lambda_1)F(\Lambda_2) \rangle \approx \Lambda_1(1 - \delta\Lambda/\Lambda_\mu), \quad \delta\Lambda \ll 1. \quad (3.16a)$$

However, when one does not have homogeneity, it is more conventional to work with the normalized two-point correlation function

$$\psi(\Lambda_1, \Lambda_2) \equiv \frac{\langle F(\Lambda_1)F(\Lambda_2) \rangle}{[\langle F^2(\Lambda_1) \rangle \langle F^2(\Lambda_2) \rangle]^{1/2}}. \quad (3.16b)$$

If we expand ψ in $\delta\Lambda$, then the first-order term vanishes, and we have

$$\psi(\Lambda + \delta\Lambda, \Lambda) \approx 1 - \frac{1}{2} \frac{(\delta\Lambda)^2}{\Lambda_c^2}, \quad \delta\Lambda \ll 1; \quad (3.16c)$$

hence, Λ_c is a coherence scale in the conventional sense.

For sharp k -space filtering, Λ_c vanishes; thus, both $\langle R_{\text{up}} \rangle$ and $\langle R_{\text{down}} \rangle$ are infinite. This is not surprising for, as the resolution interval $\Delta \ln k$ decreases, the trajectories become progressively more jittery. Hence around any point on the $F = f_v$ boundary, there will be infinitely many crossings. What is finite is the difference between up- and downcrossing points. Since ups and downs will come in pairs with arbitrarily close spacings, the first upcrossing rate will be exactly $R_{\text{up}} - R_{\text{down}}$. Indeed we do get the Press-Schechter formula complete with the factor of 2 from equation (3.14c) if we use $\langle F dF/dR \rangle = 2\sigma d\sigma/dR$, i.e., $\Lambda_\mu = \Lambda$. (That the coherence length Λ_c vanishes for sharp k -space filtering is a reflection of the nondifferentiability of

$$\psi(\Lambda_1, \Lambda_2) = (1 + \delta\Lambda)^{-1/2} [1 + \theta(-\delta\Lambda)\delta\Lambda/\Lambda]$$

in this case.)

For all filters other than sharp k -space, $\Lambda_\mu = 2\Lambda$; hence, the Press-Schechter formula *without the factor of 2* is obtained for $\langle R_{\text{up}} - R_{\text{down}} \rangle$. This is especially easy to see since, for non-sharp- k space filters, we have precisely

$$N_{\text{ud}}(\Lambda) = \theta(F - f_v). \quad (3.17)$$

Thus $\langle N_{\text{ud}}(\Lambda) \rangle = P[F(\Lambda) > f_v]$ is the probability that the field value is above threshold.

The upcrossing probability now is not infinite but will clearly give an overestimate of the first upcrossing rate. For Gaussian filtering, the correlation length

$$\Lambda_c = 2\Lambda\gamma(1 - \gamma^2)^{-1/2} \quad (3.18a)$$

is expressible in terms of the standard spectral measure γ defined in BBKS by the equations

$$\gamma \equiv \frac{\langle k^2 \rangle}{\langle k^4 \rangle^{1/2}} = \frac{\sigma_1^2}{\sigma_2 \sigma_0}, \quad (3.18b)$$

$$\sigma_j^2(R_f) \equiv \int d \ln k k^{2j} \mathcal{P}_\rho(\ln k) \exp(-k^2 R_f^2). \quad (3.18c)$$

However, for top hat filtering the evaluation of Λ_c involves other integrals that must be calculated numerically.

3.2.3. The First Upcrossing Rate—General Formalism

What we would really like to evaluate is the average $\langle R_{1\text{up}} \rangle$, given by equation (3.13). We can derive a general expression for it which will illustrate why an analytic solution is not feasible. For this, an alternative way of expressing (3.13) in operator form is more useful:

$$R_{1\text{up}}(\mathbf{r}, \Lambda) = R_{\text{up}}(\mathbf{r}, \Lambda) \{1 - \theta[N_{\text{up}}(\mathbf{r}, \Lambda -)]\}. \quad (3.19)$$

By $\Lambda -$ we mean $\Lambda - \delta\Lambda$, where $\delta\Lambda$ is positive and infinitesimal. Equation (3.19) is the form we use for the general derivation of $\langle R_{1\text{up}} \rangle$, but interpreted in a rather suggestive form. When averaged and multiplied by $\delta\Lambda$, what equation (3.19) expresses is a product of the probability that the interval from 0 to $\Lambda - \delta\Lambda$ is devoid of upcrossing points and the number of upcrossing points in the interval from $\Lambda - \delta\Lambda$ to Λ . For sufficiently small $\delta\Lambda$, the latter is the probability that the infinitesimal interval has at least one upcrossing point. Recalling the way one can treat voids in a Gaussian random field (e.g., White 1979), it may not be surprising that this can be expressed in terms of the derivative with respect to Λ of the probability there is a void of upcrossing points in resolution

space from 0 to Λ :

$$\langle R_{1\text{up}}(\Lambda) \rangle = -\frac{\partial}{\partial \Lambda} P_{\text{no up}}(\Lambda), \quad P_{\text{no up}} = 1 - \langle N_{1\text{up}}(\mathbf{r}, \Lambda, f_v) \rangle. \quad (3.20)$$

The void probability is obtained by taking the limit, giving the usual expression

$$P_{\text{no up}} = \exp \left[\sum_{M=1}^{\infty} \frac{(-1)^M}{M!} \langle N_{\text{up}}^M \rangle_{\text{cc}} \right],$$

$$\langle N_{\text{up}}^M \rangle_{\text{cc}} \equiv \int_0^{\Lambda} d\Lambda_1 \langle R_{\text{up}}(\Lambda_1) \rangle \dots \int_0^{\Lambda} d\Lambda_M \langle R_{\text{up}}(\Lambda_M) \rangle \zeta^{(M)}(\Lambda_1, \dots, \Lambda_M). \quad (3.21)$$

Here $\zeta^{(M)}$ is the reduced continuous M -point correlation function of R_{up} . The mean of the 1-up density is

$$\langle R_{1\text{up}}(\Lambda) \rangle \delta \Lambda = \delta \Lambda \sum_{M=0}^{\infty} \frac{(-1)^M}{(M)!} \langle R_{\text{up}}(\Lambda) N_{\text{up}}^M(\Lambda) \rangle_{\text{cc}} \exp \left[\sum_{M=1}^{\infty} \frac{(-1)^M}{M!} \langle N_{\text{up}}^M(\Lambda) \rangle_{\text{cc}} \right]$$

$$= \delta \Lambda \langle R_{\text{up}} e^{N_{\text{up}}} \rangle_{\text{cc}} \exp [-\langle 1 - \exp (-N_{\text{up}}) \rangle]. \quad (3.22)$$

The last expression is a purely formal mnemonic for remembering the formula. It is to be understood to mean the expansion in terms of the normalized continuous connected correlation functions. These formulae are derived in the Appendix. Obviously it is a formidable task indeed to attempt to get all reduced correlation functions, and we have made very little progress on this beyond the level of the two-point function.

3.2.4. Analytic Approximations for the First Upcrossing Rate

We have found limits $\langle N_{\text{up}} \rangle$ and $\langle N_{\text{ud}} \rangle$ which bracket the exact solution $\langle N_{1\text{up}} \rangle$ for general filters, but can we do better? There is one fairly well motivated approximation, described by Peacock & Heavens (1989), that gives a relatively accurate description of the numerical results. Other analytic approximations, described in the Appendix, with specific assumptions concerning the correlation hierarchy are less well motivated and often do not fare as well. Peacock & Heavens adopted an *Ansatz* for $\langle N_{1\text{up}} \rangle$, which in our language would be

$$\langle N_{1\text{up,PH}}(\Lambda_j) \rangle \approx [1 - \langle N_{\text{ud}}(\Lambda_j) \rangle] \prod_{i=1}^{j-1} [1 - \langle N_{\text{ud}}(\Lambda_i) \rangle]. \quad (3.23)$$

They supposed the resolution intervals $\delta \Lambda_i = \Lambda_i - \Lambda_{i-1}$ could be chosen just large enough so that the trajectories in each interval would be effectively uncorrelated with the adjacent ones. They introduced a correlation length Λ_{PH} to describe the required step. For Gaussian filtering, it is proportional to the coherence scale introduced in § 3.3.1:

$$\Lambda_{\text{PH}} = (\pi \ln 2) \Lambda_c. \quad (3.24)$$

They then took a continuum limit of the product (3.23):

$$P_{\text{no up,PH}}(\Lambda) = [1 - \langle N_{\text{ud}}(\Lambda) \rangle] \exp \left\{ - \int_0^{\Lambda} \ln [1 - \langle N_{\text{ud}}(\Lambda') \rangle]^{-1} \frac{d\Lambda'}{\Lambda_{\text{PH}}(\Lambda')} \right\}. \quad (3.25)$$

Differentiating yields the Peacock & Heavens approximation to $\langle R_{1\text{up}} \rangle$:

$$\langle R_{1\text{up,PH}} \rangle(\Lambda) \approx [\langle R_{\text{ud}} \rangle + (1 - \langle N_{\text{ud}} \rangle) \ln (1 - \langle N_{\text{ud}} \rangle) \Lambda_{\text{PH}}^{-1}] \left[1 - \exp \left\{ - \int_0^{\Lambda} \ln [1 - \langle N_{\text{ud}}(\Lambda') \rangle]^{-1} \frac{d\Lambda'}{\Lambda_{\text{PH}}(\Lambda')} \right\} \right]. \quad (3.26)$$

It does well asymptotically on the faint side, as can be seen from Figure 5. However, it overshoots the peak somewhat. We also show the quantity $-d \exp [-\langle N_{\text{up}}(\Lambda) \rangle]/d \ln M$ in Figure 5, which arises if we ignore all reduced correlation functions except for the one-point functions in equation (3.21). It does reasonably well for the CDM case but does not fare as well as the Peacock-Heavens approximation for the power law results in Figure 9.

4. COMPARISON OF EXCURSION SET THEORY WITH N -BODY RESULTS

In the previous section we have discussed solutions to the mass functions for various choices of filter function. In the case of a sharp k -space filter, our solution gives exactly the Press-Schechter formula. However, we find that the shape of the multiplicity function depends on the choice of the filter function. As our numerical solutions demonstrate, Gaussian and top hat filter functions give fewer high-mass objects and more low-mass objects than the Press-Schechter formula. The differences between these curves are small near the knee of the mass-function at the characteristic mass M_* but become large at the low-mass end.

How are we to interpret these differences? There is no compelling theoretical reason to favor one form of filter function over another, and so it seems more likely that the sensitivity to the form of the filter-function indicates that the excursion set approach provides a poor model for the formation and evolution of low-mass structures. In this section, we compare the predicted mass functions with results from N -body simulations. We already know from previous work (e.g., Efstathiou et al. 1988) that the Press-Schechter formula provides a reasonable fit to the N -body mass-functions, though it is of interest to check whether the results

for other filter functions provide acceptable fits. Of more interest, however, is to investigate just how well particles in non-linear clumps can be identified with excursion sets in the initial conditions.

The simulations used here are the scale-free models described in the paper by Efstathiou et al. (1988). These simulations begin with Gaussian initial fluctuations with power-law power spectra (eq. [3.6c]), $\mathcal{P}_\rho(k) \propto k^{3+n}$, superposed on a flat $\Omega = 1$ background. Here we examine the simulations with spectral index $n = -2, -1$, and $+1$, providing a wide range of initial conditions.

We produced smoothed versions of the N -body initial conditions by convolving the initial density field with a set of filters with closely spaced radii R_f . At the initial position of each particle in the simulation, we stepped through the set of filters, starting with the filter with the largest R_f , continuing until the smoothed density at this point exceeding the threshold value of f_v/a , at which point we assign the filter mass $M(R_f)$ to this particle. Here a is the factor by which the universe has expanded since the start of the simulation and equals the factor by which the linear theory density field has grown. To assign a mass to each particle we must adopt a mass-filter radius relation $M(R_f)$ and a value for the linear density threshold f_v , at which we assume a virialized object to have formed. Once these choices have been made, this prescription leads precisely to the corresponding cumulative mass functions $\Omega(>R_f)$ that we calculated in § 3.

For the threshold we choose $f_v = 1.686$, which is the linear theory overdensity of a spherical top hat perturbation which has just collapsed to a singularity (see, e.g., BBKS). For the case of top hat filtering, the $M(R_f)$ relation we adopted was simply the mass contained within the filter,

$$M = \frac{4\pi}{3} \Omega \rho_{\text{cr}} R_{\text{TH}}^3 . \quad (4.1)$$

For other filtering choices, we fixed the relation between R_f and R_{TH} by requiring that the relation $M(\Lambda)$ be independent of the choice of filter function. Equations (2.2) and (2.3) then determine the relation between R_{TH} and R_f for other filters and so determine the $M(R_f)$ relation. For power-law spectra and Gaussian filtering, this yields $R_f \approx (0.45-0.5)R_{\text{TH}}$, with little sensitivity to the spectral index n . In earlier work, Bond (1988a) adopted $R_f \approx 0.43R_{\text{TH}}$, and argued that $0.38 \lesssim R_f/R_{\text{TH}} \lesssim 0.64$. From scaling arguments one can show that $M \propto \Lambda^{-3/(n+3)}$, but what to choose for the constant of proportionality for each filter is debatable. Choosing different constants for the different filters would have the effect of horizontally displacing the curves of Figure 5 (and Fig. 9 below) by different amounts. As we shall see, the N -body data we have used are unable to determine how best to tune the $M(R_f)$ relation. However, we stress that in order to accurately predict the abundance of rare massive clusters, the $M(R_f)$ relation must be accurately calibrated.

To compare these mass assignments to the results of the N -body simulations we used a friends-of-friends percolation algorithm (see Davis et al. 1985) to construct group catalogs at the final time in each of the N -body simulations. A link parameter of $b = 0.2$ times the mean interparticle separation was used, as this selects groups approximately bounded by an isodensity contour of about 100, which has been found to delineate roughly the boundary between virialized halos and surrounding infalling material. The majority of groups defined in this way contain one dominant density center, but occasionally percolation selects a group with two or more distinct density centers joined by tenuous bridges. Furthermore, one should ignore groups with contain only a few particles which are often found in the outer halos of very massive groups due to purely statistical fluctuations in the poorly sampled density field. Thus these group catalogs should not be viewed as the definitive way of selecting and classifying virialized halos.

Having done this for the whole simulation, we can compare the filter masses assigned to each particle with the mass of the group in which the particles are actually found at the end of the simulation as illustrated in Figures 6 and 7. Figure 6a shows the regions of space occupied by the initial density perturbations which collapse to form massive groups in one of the simulations. The regions predicted to end up in groups of the same mass range are shown in Figures 6b and 6c for sharp k -space and Gaussian filters respectively. One can see that for both of these filter functions, the regions selected correspond roughly with those in Figure 6a. There is a void running up the center of the box, with the largest structures forming from material initially at the edges of the box. The filter schemes tend to miss the outer regions of some of the density perturbations and also form bridges between them. The final positions of each of these sets of particles are shown in Figures 7a-7d. One can see that the massive groups identified in the N -body simulation (Fig. 7a) are in general well represented in both Figures 7b and 7c, indicating a reasonably good correspondence between the sets of particles selected by the filtering schemes and the set of particles we would have liked to have identified. However, one can find many examples of particles selected by the filtering schemes which end up in lower mass groups (such as the group one-fourth of the way up the left-hand edge of Figs. 7b and 7c) whose masses are not large enough for the group to be plotted in Figure 7a. Also, the particles residing in the bridges identified in Figures 6b and 6c often do not end up in massive groups at all. Together this produces a large scatter in the ratio of assigned filter mass to actual group mass.

The corresponding plots for lower mass groups are shown in Figures 6d-6f and Figures 7d-7f. Here the degree of correspondence between the regions of space occupied by the density perturbations, which form the low-mass groups, and regions of space selected by our filtering schemes, is far worse. Comparison of Figures 6f and 6d reveals that the Gaussian filter has selected some of the groups that form in the N -body simulation, but overall the correspondence is not good.

As well as the Gaussian and sharp k -space filter functions used to produce Figures 6 and 7, we also used a real space top hat filter function, and for each we tried a range of threshold values. The exact correspondence between the filtering scheme and the N -body simulation depends somewhat on the form of filter function used and the threshold, but we did not find the degree of agreement to be noticeably better for any one particular choice.

Detailed comparisons have shown that two effects lead to the poor agreement between the mass assigned by the filtering scheme and the mass of group that the particles end up in. First, there is a tendency to pick up the cores of small groups when filtering on a mass scale somewhat larger than the group mass, and a related tendency not to pick up the wings of a group until the filter mass is significantly smaller than the group mass. Second, for any perturbation the boundary of the particles selected by the filtering scheme

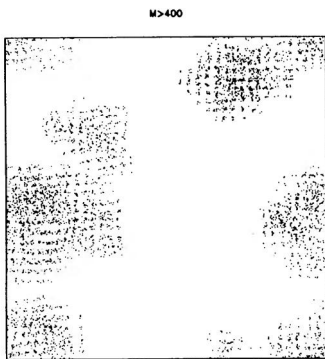


FIG. 6a

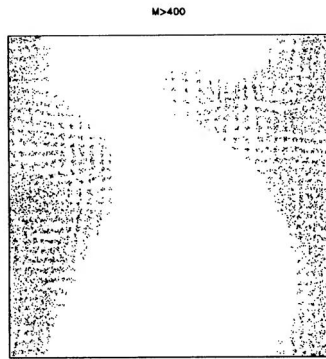


FIG. 6b

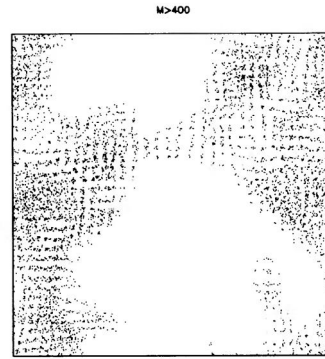


FIG. 6c

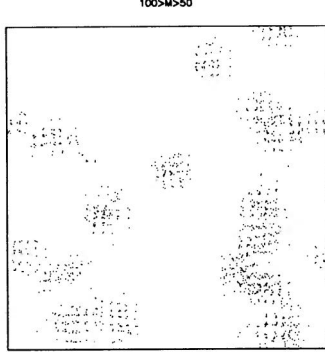


FIG. 6d

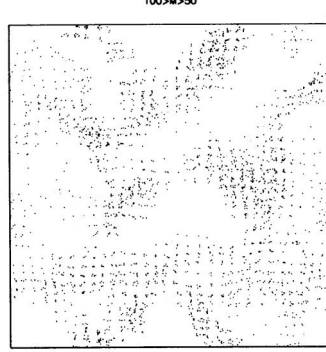


FIG. 6e

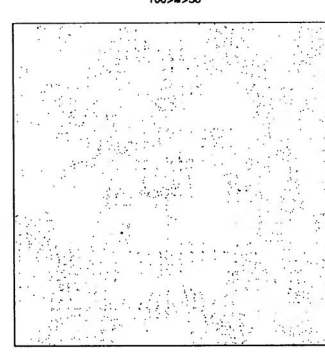


FIG. 6f

FIG. 6.—Shown are the initial positions of various subsets of particles in one of the N -body simulations, which started from initial conditions with spectral index $n = -2$. The particles plotted in (a) and (d) are those particles in the N -body simulation which end up in groups with masses in the range indicated above the figures. Figures (b) and (e) show the subset of particles that are assigned a filter mass in the same range when using a sharp k -space set of filters and (c) and (f) result from using a set of Gaussian filters.

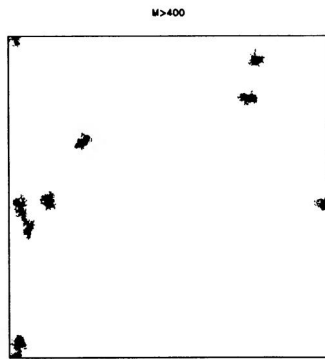


FIG. 7a

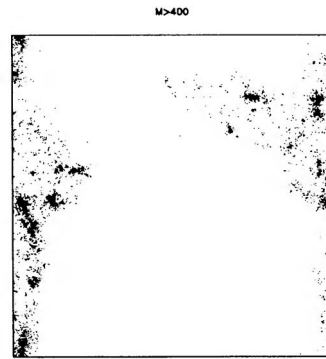


FIG. 7b

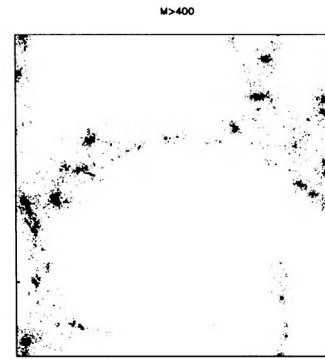


FIG. 7c

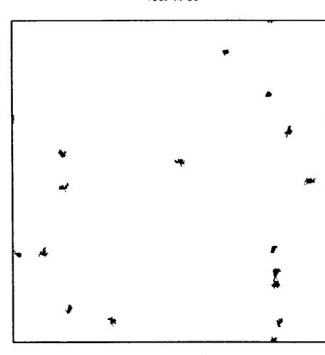


FIG. 7d

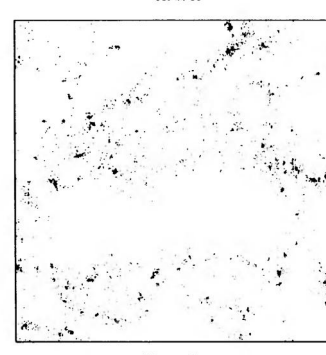


FIG. 7e

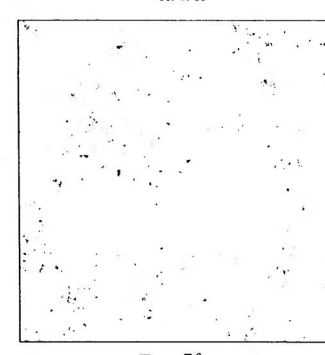


FIG. 7f

FIG. 7.—These figures show the same particles as the corresponding plots of Fig. 6. The only difference is that here the particles are plotted at their final positions in the N -body simulation rather than at their initial positions.

EXCURSION SET MASS FUNCTIONS

453

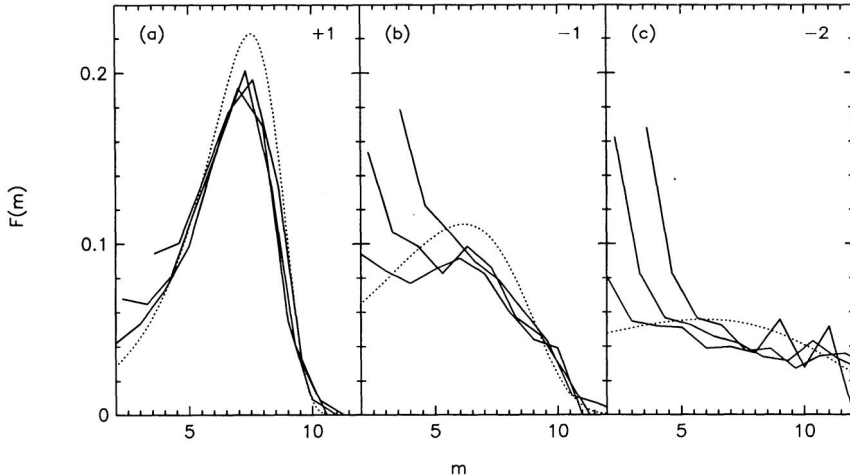


FIG. 8.— $F(m)$ is the fraction of mass in groups of multiplicity m . The multiplicity of a group of N particles is defined by $2^m \leq N < 2^{(m+1)}$ particles. We have plotted the multiplicity functions of the last three output times for each ensemble of simulations. The multiplicities of groups at the earlier times have been scaled to match those at later times by the self-similar scaling $M_* \propto a^{6/(3+n)}$. Figures (a)–(c) show results for the spectral indices +1, -1, and -2, respectively. The dotted lines show the Press-Schechter formula. The curves extracted from the N -body simulations turn up at low masses due to the discreteness limit of the simulation.

will differ from that defined by the particles which end up in the N -body group. This is inevitable as the filtered density field is sensitive to surrounding perturbations. Thus, when filtering on a mass scale $M \gtrsim M_*$, we get reasonable correspondence between the regions our filtering scheme selects and the regions which actually form groups of the corresponding mass in the N -body simulation. For $M \ll M_*$, where objects are constructed out of the mass left over by the larger objects, the filtering scheme understandably shows little correspondence with the N -body simulations.

This problem is inevitable in any local filtering scheme, and cannot be avoided by judicious choice of filtering function. Any local filtering scheme will necessarily have problems selecting particles at the edge of a density perturbation, since, when the filter is offset from the center of the perturbation, it will not feel the full contribution of the perturbation. Thus particles in the wings of groups are likely to be assigned masses significantly less than the group mass. Also it is unlikely that any filtering scheme will be able to identify those particles which end up in groups with $M \ll M_*$, since here it is very much a matter of mopping up the mass left over from the formation of the larger groups.

As well as the above detailed comparison with individual simulations, we used the $b = 0.2$ percolation group catalogs to extract various statistical properties from each ensemble of N -body simulations. The mass functions for the ensembles with $n = -2, -1$, and +1 are shown in Figure 8. Despite the poor particle-by-particle comparison detailed above, the mean mass functions follow remarkably well the sharp k -space (Press-Schechter) mass function.

Figure 9 compares the mass functions calculated numerically by generating Langevin trajectories for Gaussian and top hat filters with the Press-Schechter result. These differ by a factor 2 in the asymptotic rare high-mass end and have significantly different low-mass slopes. However, comparing with Figure 8 we see that over the limited mass range probed by the N -body simulations,

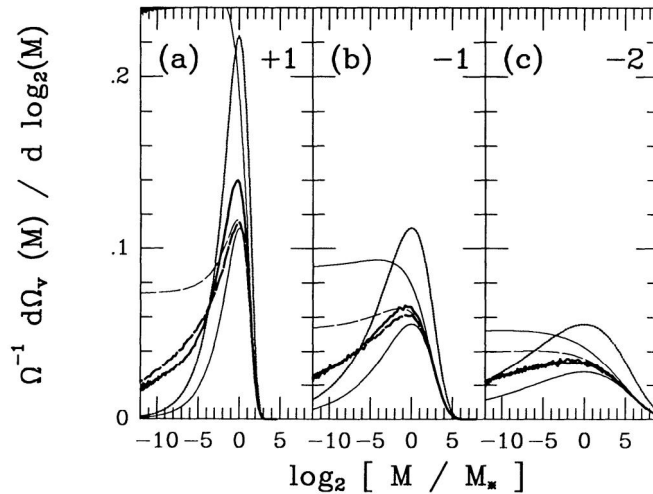


FIG. 9.—Monte Carlo computations of the first upcrossing rate for top hat (heavy solid) and Gaussian (dashed) filtering are compared with the sharp k -space Press-Schechter formula (dotted). 10^6 paths were computed for each case. The analytic upper bound $d\langle N_{up} \rangle / d \log_2 M$ and the “up minus down” rate $d\langle N_{ud} \rangle / d \log_2 M$ are shown by the lighter lines. The latter is the same for both filters and is one-half of the PS formula. The base 2 logarithm was chosen for direct comparison with the N -body results of Figure 8.

they also provide adequate fits to the data. The Press-Schechter result overestimates the mass function by as much as 20% at the peak while the mass functions for less spatially extended filters underestimate the height of the peak by a comparable amount.

These comparisons show that the excursion set approach provides a reasonable, though by no means flawless, description of the formation of massive groups in the N -body simulations. However, the approach rapidly breaks down for groups of mass $\ll M_*$ where we find an extremely poor correspondence between low-mass groups and overdense regions in the initial conditions. The differences between the slopes of the mass-functions at the low-mass end predicted for different filter function slopes are thus probably only of academic interest and not of much relevance to the formation of low-mass groups. Over the range $M \gtrsim M_*$, where the excursion set theory certainly is relevant to group formation, the predicted mass-functions are relatively insensitive to the choice of filter function and are in good agreement with the N -body simulations.

This may seem unsatisfactory, since it demonstrates that we have no theoretical framework for calculating the shape of the multiplicity function at low mass. However, to do so, we would have to abandon the excursion set approach and adopt nonlocal criteria for the formation of structure, say by locating mass around peaks in the initial density field. Such nonlocal criteria are not only extremely hard to work with analytically, but would probably have to be fairly elaborate to describe the formation of low-mass objects accurately (for example, we would probably have to consider cloud shapes and proximity to massive systems). Until such an improved theory is developed, one should be cautious about applying the Press-Schechter formula for mass-scales outside the range that has been tested in N -body simulations, especially at the low-mass end.

From the above remarks it may seem as though the formalism developed in § 3 is of limited use. In fact, we show in the next section that it is a much more powerful approach than the Press-Schechter theory since it can be adapted to calculate more complicated quantities than the overall multiplicity function. For example, our formalism can describe mergers of groups and the shape of the mass-function in special regions. As above, we would not expect these results to apply to objects of mass $\ll M_*$, but we would expect a reasonable correspondence for more massive groups as indeed we find to be the case.

5. MERGERS AS A TWO BARRIER ABSORPTION PROBLEM

In § 3 we calculated the fraction of trajectories of $F(\mathbf{r}, \Lambda)$ that make their first upcrossing through the threshold $f_v/D(z)$ at resolution $\Lambda(M)$ and interpreted this as the fraction of mass that is incorporated in objects of the mass M at redshift z . Using this same formalism, it is clear that we can relate the mass distribution of objects at two redshifts z_1 and z_2 by considering two thresholds at $f_{v1} = f_v/D(z_1)$ and $f_{v2} = f_v/D(z_2)$. Here we consider the fraction of trajectories which make their first upcrossing of the lower threshold f_{v2} at resolution $\Lambda(M_2)$, and then upcross through the higher threshold f_{v1} for the first time at $\Lambda(M_1)$. We interpret this as the fraction of mass that was in objects of mass M_1 at z_1 that is later in objects of mass M_2 at z_2 . Knowledge of this quantity makes it possible to calculate many statistics concerning the merging of objects. In the following sections, we calculate $n(M_1, z_1 | M_2, z_2)$, the number of objects of mass M_1 at redshift z_1 which by redshift z_2 have merged and been incorporated in objects of mass greater than M_2 . Once again, analytic results can be obtained for sharp k -space filtering (§ 5.1), but Monte Carlo calculations are needed for Gaussian and top hat filtering (§ 5.2). This constrained number density gives the multiplicity function for regions destined to become clusters of mass greater than M_2 at redshift z_2 . By comparing with the average multiplicity function at the earlier redshift z_1 , we can measure the “bias” in the mass distribution of objects in protoclusters, finding that massive clusters are built from the most massive objects present at z_1 . As in previous sections, we compare these results with N -body simulations.

5.1. Merger Probabilities for Sharp k -Space Filters

For sharp k -space filtering, $F(\mathbf{r}, \Lambda)$ is a Markov variable, dependent only upon its most recent value rather than on the past history. Thus, for $\Lambda > \Lambda_2$, the constrained trajectory which equals f_{v2} at Λ_2 is just f_{v2} plus the solution of the Langevin equation (3.6) for the variable $F - F_2$ in the resolution variable $\Lambda - \Lambda_2$, which vanishes at $\Lambda - \Lambda_2 = 0$. If we are interested in trajectories which pass through f_{v2} at Λ_2 and are absorbed at a second higher barrier f_{v1} , we need solve only for these constrained trajectories. As in § 3.1, solving the diffusion equation (3.5) is the simpler approach. The solution $\Pi(F, \Lambda | \Lambda_2, f_{v2})$ for the constrained probability of F at Λ given f_{v2} at Λ_2 can then be expressed in terms of the solution (3.1) of equation (3.5), but in the variables $F - F_2$ and $\Lambda - \Lambda_2$: $\Pi(F - f_{v2}, \Lambda - \Lambda_2, f_{v1} - f_{v2})$. The constrained mass fraction is then similar to equation (3.9): of the matter which at redshift z_2 is in objects of mass M_2 , the fraction which was in objects of mass M_1 at redshift z_1 is

$$\frac{1}{\Omega} \frac{d\Omega_v}{d \ln M_1} (M_1, z_1 | M_2, z_2) = \frac{1}{\sqrt{2\pi}} \frac{(f_{v1} - f_{v2})}{(\Lambda_1 - \Lambda_2)^{1/2}} \exp \left[-\frac{(f_{v1} - f_{v2})^2}{2(\Lambda_1 - \Lambda_2)} \right] \frac{d \ln (\Lambda_1 - \Lambda_2)}{d \ln M_1} \delta(\Lambda_1 - \Lambda_2). \quad (5.1)$$

The δ function ensures that only objects of mass M_1 below M_2 can reside in the cluster of mass M_2 which virializes at redshift z_2 .

Equation (5.1) is precisely the answer one would have found had one used the Press-Schechter approach (taking the derivative with respect to Λ_1) of the fraction of points at resolution Λ_1 with amplitude in excess of f_{v1} subject to the constraint that, on the lower resolution scale Λ_2 , the field had value f_{v2} . Of course a fudge factor of 2 would have to be applied. How the analog of equation (5.1) is obtained for the general case is described in § 5.2.

To provide a comparison with the N -body simulations, we calculate the cumulative quantity:

$$\frac{1}{\Omega} \frac{d\Omega_v}{d \ln M_1} (M_1, z_1 | > M_2, z_2) = \int_0^{\max(M_1, M_2)} dM'_2 \frac{1}{\Omega} \frac{d\Omega_v}{d \ln M_1} (M_1, z_1 | M'_2, z_2) \frac{1}{\Omega} \frac{d\Omega_v}{d \ln M_2} (M'_2, z_2). \quad (5.2)$$

Although this equation can be simplified somewhat, it still must be integrated numerically. In Figures 10, 11, and 12 we compare the results of the multiplicity function for power-law runs with this formula. It appears to fit the simulation data remarkably well.

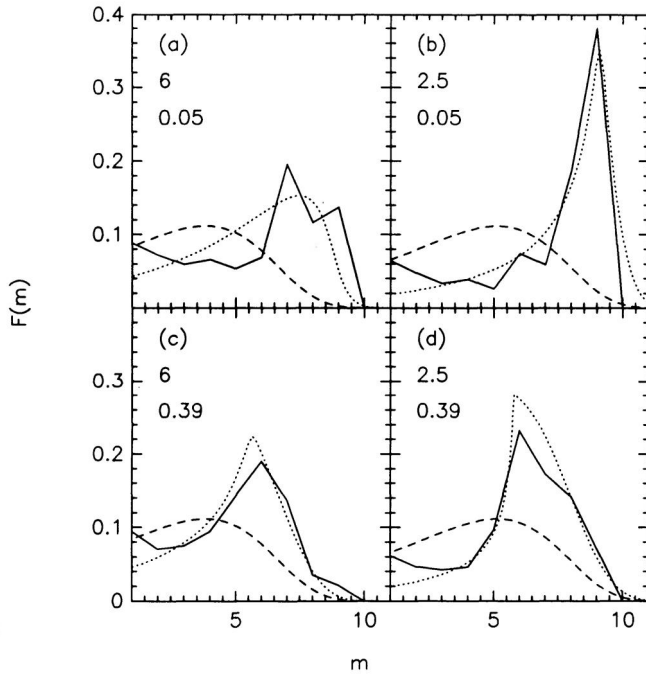


FIG. 10.—Multiplicity functions of particles that end up in massive groups in the $n = +1$ simulations compared with the solutions of the two absorbing barrier problem (eq. [5.2]). In each case we located groups at the final output time and selected particles in the most massive groups containing 0.05 (a and b) and 0.39 (c and d) of the total mass. The multiplicity functions for these subsets of particles are shown at earlier times when m_* was smaller by a factor of 2.5 (b and d) and by a factor of 6 (a and c). The predictions of the two absorbing barrier problem are shown as the dotted line. The multiplicity function for an average region of space (eq. [3.9]) is shown by the dashed line. As in Fig. 8, the turn up at low masses of the curves extracted from the N -body simulations is an artifact of the discreteness of the simulation.

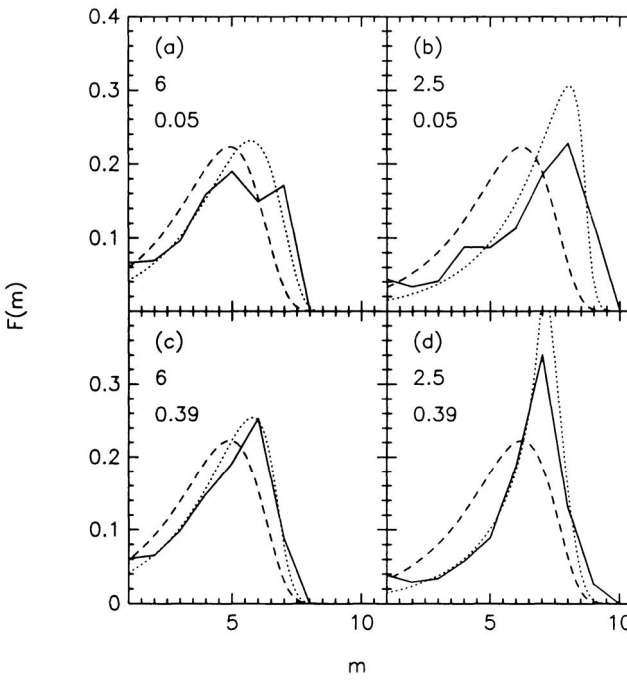


FIG. 11.—As Fig. 10 but for the $n = -1$ simulations

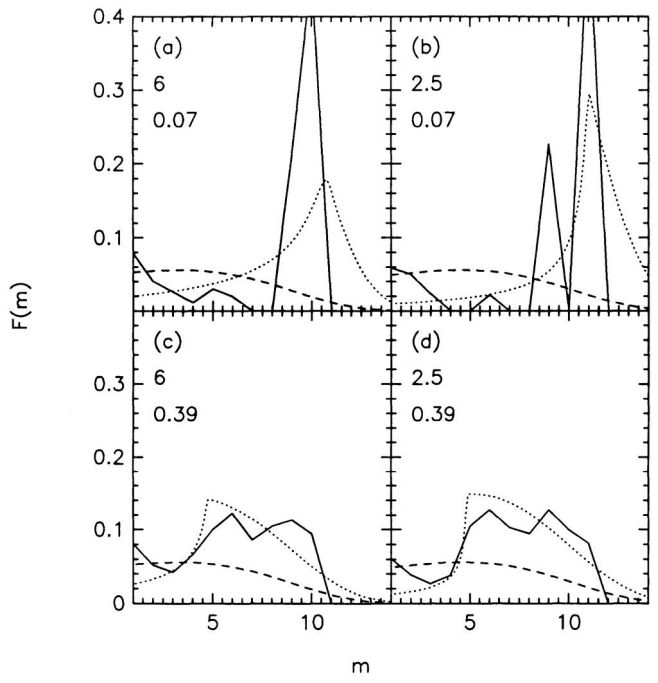


FIG. 12.—As Fig. 10 but for the $n = -2$ simulations

5.2. Merger Probabilities for General Filters

We can express the merger rate (5.1) for general filters in terms of a correlation function of the first upcrossing rate at contour level f_{v2} , $R_{1\text{up}}(\Lambda_2, f_{v2})$, and the first upcrossing rate at contour level f_{v1} , $R_{1\text{up}}(\Lambda_1, f_{v1})$:

$$\frac{1}{\Omega} \frac{d\Omega_v}{d \ln M_1} (M_1, z_1 | M_2, z_2) = \frac{\langle R_{1\text{up}}(\Lambda_1, f_{v1}) R_{1\text{up}}(\Lambda_2, f_{v2}) \rangle}{\langle R_{1\text{up}}(\Lambda_2, f_{v2}) \rangle} \frac{d\Lambda_1}{d \ln M_1}. \quad (5.3)$$

The straightforward way to calculate this ratio is to perform a Monte Carlo simulation, using a large number, N_{paths} , of paths. The operational procedure is as follows. Assume Λ -space is split into bins $(\Lambda_{j-1}, \Lambda_j)$. We use bins spaced according to the prescription of § 3.2. We estimate the correlation function by forming the sum

$$\langle R_{1\text{up}}(\Lambda_j, f_{v1}) \delta\Lambda_j R_{1\text{up}}(\Lambda_i, f_{v2}) \delta\Lambda_i \rangle = \frac{1}{N_{\text{paths}}} \sum_{\text{paths}} [N_{1\text{up}}(\Lambda_j, f_{v1}) - N_{1\text{up}}(\Lambda_{j-1}, f_{v1})][N_{1\text{up}}(\Lambda_i, f_{v2}) - N_{1\text{up}}(\Lambda_{i-1}, f_{v2})]. \quad (5.4)$$

For each trajectory, the product of $N_{1\text{up}}$ differences in equation (5.4) vanishes unless the path first crossed through f_{v1} in the $(\Lambda_{j-1}, \Lambda_j)$ interval and through f_{v2} in the $(\Lambda_{i-1}, \Lambda_i)$ interval, in which case the product is unity. Since the fraction which upcrosses through f_{v2} in $(\Lambda_{i-1}, \Lambda_i)$ is estimated from

$$\langle R_{1\text{up}}(\Lambda_i, f_{v2}) \delta\Lambda_i \rangle = \frac{1}{N_{\text{paths}}} \sum_{\text{paths}} [N_{1\text{up}}(\Lambda_i, f_{v2}) - N_{1\text{up}}(\Lambda_{i-1}, f_{v2})], \quad (5.5)$$

we obtain an estimate of equation (5.3) by taking the ratio of equations (5.4) and (5.5). Since we are often interested in other constrained averages, such as equation (5.2), we form the ratios only after appropriate summation over the i bins.

In developing approximations to merger formulas, it is often most convenient to work with integral quantities such as

$$\Omega_v(>M_1, f_{v1} | >M_2, f_{v2}) = \frac{\langle N_{1\text{up}}(\Lambda_1, f_{v1}) N_{1\text{up}}(\Lambda_2, f_{v2}) \rangle}{\langle N_{1\text{up}}(\Lambda_2, f_{v2}) \rangle}. \quad (5.6)$$

This is especially true for the $N_{\text{ud}} = N_{\text{up}} - N_{\text{down}}$ approximation, since, for filters other than sharp k -space, the operator N_{ud} is simply $\theta(F_\Lambda - f_v)$ (eq. [3.17]). Thus, to form the “ud” approximation, we need only differentiate

$$\Omega_v(>M_1, f_{v1} | >M_2, f_{v2}) = \psi_{\text{PS}} P(F_1 > f_{v1} | F_2 > f_{v2}) \quad (5.7)$$

with respect to M_1 , where P is an integral conditional probability derived from the usual “peak-background” split differential constrained probability for field points given in Appendix E of BBKS:

$$\begin{aligned} P(F_1, \Lambda_1 | F_2, \Lambda_2) dF_1 &= \frac{1}{\sqrt{2\pi}} e^{-v_p^2/2} dv_p, \quad v_p \equiv \frac{[F_1 - (\Lambda_h/\Lambda_1)F_2]}{(\Lambda_1 - \Lambda_h^2/\Lambda_2)^{1/2}}, \\ \Lambda_h &= \int \tilde{W}(kR_{\Lambda_1}) \tilde{W}(kR_{\Lambda_2}) \mathcal{P}_\rho(k) d\ln k. \end{aligned} \quad (5.8)$$

Equation (5.7) is of course what one would get if one followed the standard Press-Schechter approach; and although the fundge factor ψ_{PS} is naturally unity, we could arbitrarily take it to be 2, as in the unconstrained case. However, the quantity Λ_h is not equal to Λ_2 except for the case of sharp k -space filtering, so the PS approximation differs for different filters. Further, we are now no longer guaranteed that the integral quantity (5.7) is a lower bound to the exact result, since we divide by $\langle N_{\text{ud}}(\Lambda_2, f_{v2}) \rangle$. However, we expect that it will be a good approximation on the rare event side.

In Figures 13, 14, and 15 we compare numerical estimates of this merger multiplicity function evaluated by tracing Langevin trajectories with the analytic sharp k -space filter formula of § 5.1. The shape for top hat and Gaussian filterings are quite similar but differ noticeably from the sharp k -space form. Thus, unlike the situation in § 4, where the average multiplicity function determined from N -body simulation data was well described by all filtering types, comparison with Figures 10, 11, and 12 show that the k -space filter formula is somewhat preferred.

Although the calculations shown have a very wide spread in wavenumber, the $32^3 N$ -body runs shown here only vary over a factor of 16 in wavenumber. We performed Monte Carlo simulations for these limited band cases and find that the biggest effect occurs for $n = -2$. Figure 14 for $n = -1$ is only slightly altered so the conclusion that the sharp k -space formula is slightly preferred remains. For $n = -2$, the plateau of Figure 15d is greatly rounded, making the discrepancy between the predictions for the various filters only slightly favoring the sharp k -space formula, rather than the strong differentiation indicated with a broader band in k -space. The mean multiplicity calculations of Figure 9 have the low-mass tails for the Gaussian and top hat filtering functions severely curtailed, which strengthens the conclusion that the N -body calculations used here can not effectively differentiate between the various formulae. These tail truncations are in large part a result of the low-mass flattening of the σ_ρ - M relation.

6. DISCUSSION

We have constructed simple models for the mass function of virialized clumps based on the statistics of critical density excursion sets as a function of resolution. Our model is similar to that of Press & Schechter but is intended to improve on their analysis by a more realistic treatment of the cloud-in-cloud problem. In our view, Press & Schechter made a false assumption in that they implicitly assumed that underdense regions cannot be embedded in larger regions with a higher mean density. This is clearly not

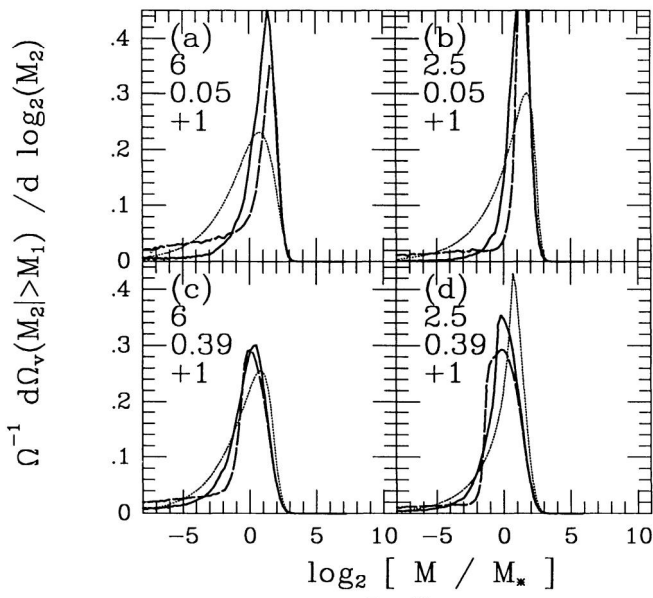


FIG. 13

FIG. 13.—The analytic sharp k -space result (dotted line) for the proto-cluster mass function is compared with the Monte Carlo results for top hat (solid) and Gaussian (dashed) filters, using 10^6 trajectories as in Fig. 9. These figures are for spectral index $n = +1$ and the cluster mass and epochs used in Figs. 13a, 13b, 13c, and 13d correspond with those in Figs. 10a, 10b, 10c, and 10d. Comparison of these curves with those of Fig. 10 reveals that all three functions would fit the N -body results reasonably well.

FIG. 14.—As Fig. 13 but for $n = -1$ and with the cluster mass and epoch matching those of Figs. 11a, 11b, 11c, and 11d. The sharp k -space results fit the N -body data better than the top hat and Gaussian results.

true for a Gaussian random field, and it is for this reason that they were forced to introduce a factor of 2 to renormalize their multiplicity function and ensure that all the mass in the universe was accounted for. We have constructed models using various choices for the filter profile and have compared our results with groups found in N -body simulations.

For a particular choice of filter, namely a sharp filter in k -space, the variation of overdensity $F(r, R_f)$ with filter mass $M(R_f)$ is a Brownian random walk. In this case we obtain an analytic solution, identical to the Press-Schechter formula for the multiplicity function, complete with the factor of 2. What was crucial to get this Press-Schechter form with the factor of 2 was the uncorrelated nature of the steps in the random walk for sharp k -space filtering of Gaussian fluctuations. The same formalism can be applied to the random walk in number of points within a top hat radius for the case of Poisson fluctuations of the particles. Epstein (1983) formulated this Poisson problem and solved it, finding as well the fudge factor of 2, for similar reasons to those found here. Although

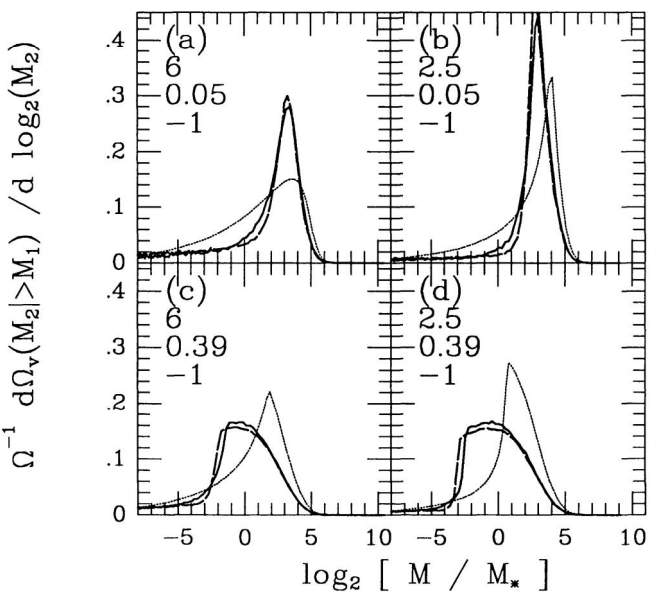


FIG. 14

a purely Poisson seed model does not include the expected large-scale evolution of the transfer function appropriate for isocurvature perturbations (see, e.g., Peebles 1987; Efstathiou & Bond 1986, 1987), so it is not a viable set of initial conditions for cosmic structure formation, the model is quite instructive as a real space analog of the random phase Gaussian fluctuation problem.

We have presented the results of numerical calculations for other (more natural) choices of filter function which have correlated random walk steps, along with analytic lower and upper bounds. We have also shown that this formalism enables the basic theory to be extended to calculate the relationship between the multiplicity function at two different epochs, enabling biases and the statistics of mergers to be studied.

We have tested the usefulness of our approach by comparison with an ensemble of N -body simulations (Efstathiou et al. 1989). We have made statistical comparisons of the mean mass functions and of the mass functions of regions destined to form massive clusters at a later time. Also, by filtering the initial Gaussian linear density field from which particular simulations were evolved, we have compared, particle by particle, the mass we assign by our filtering scheme with the mass of the group that particle resides in at the final time in the N -body simulation.

The particle-by-particle comparison with the N -body simulations reveals that the constrained excursion sets selected by our filtering scheme for a mass M only roughly coincide with the regions of Lagrangian space that collapse to form nonlinear groups of mass M . For masses $M \gtrsim M_*$, where M_* is the characteristic mass at a given epoch, we do find that particles in regions destined to form groups in the N -body simulation are assigned filter masses similar to the group mass. However, for masses $M \ll M_*$, the correspondence between assigned and group mass is very poor, which is not surprising since the points predicted to lie in low-mass objects by the excursion set theory are the leftovers from the formation of the larger groups. This is true for both sharp k -space filters and for less spatially extended filters such as Gaussian and top hat filters. Thus we must not hold much faith in the excursion set predictions for the low mass tail.

Even for masses comparable to M_* , the direct correspondence between filter mass and group mass contains a relatively large scatter. This is inevitable in any local filtering scheme, for which there are problems selecting particles at the edge of a density perturbation, since, when the filter is offset from the center of the perturbation, it will not feel the full contribution of the perturbation. Thus particles in the wings of groups are likely to be assigned masses significantly less than the group mass. From a physical point of view, it seems more natural to consider peaks of the density, up which the filter can be centered.

In spite of the detailed point by point failure of the excursion set approach, it does surprisingly well for average statistical properties such as the mass function $n(M)dM$ when compared with the statistical properties of the N -body simulations. The different filtering choices give mass functions with differing low mass slopes. However, the limited dynamical range of the N -body simulations we used to test this method prohibits the determination of the correct slope at very low masses. At the highest masses, where $n(M)$ is falling steeply, the choice of filter function changes the predicted abundance by a factor of 2, but again the poor statistics in the N -body simulations do not enable the abundance of such rare objects to be determined accurately. Over the small mass range reliably probed by the N -body simulations, the predictions for various types of filter all give results that fit the N -body data remarkably well. The sharp k -space filter, which yields the Press-Schechter mass function, overestimates the abundance of groups by as much as 20%, while the top hat and Gaussian filters yield slight underestimates. We would like to see more extensive computations of power-law models in order to more accurately test our formulae. This would help to calibrate the $M(R_f)$ relation.

While our emphasis has been mainly on testing the model mass functions, it is also of interest to compare the results with the observed galaxy luminosity function. In the popular CDM model, the Press-Schechter mass function predicts a low-mass slope which is far steeper than the almost flat faint end of the observed galaxy luminosity function. Thus, assuming an approximately constant mass-to-light ratio, one predicts a faint galaxy abundance which is far greater than is observed. This discrepancy is even larger for the mass functions resulting from other choices of filter function. However, one should remember that, for masses

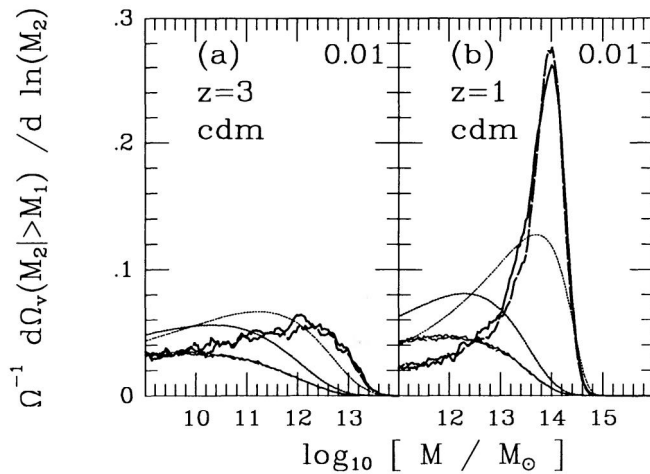


FIG. 16.—The mass function for virialized objects at redshifts 3 and 1 that merged to form rich clusters containing 1% of the matter in the universe are shown to be skewed to high mass when compared to the mass function for the typical virialized objects at those epochs. The dotted curves give the sharp k -space results, the solid gives the top hat result, and the dashed curves give the Gaussian results. 10^6 trajectories were computed for the latter, but only a small fraction of those actually hit the $z = 0$ threshold for these rare clusters. The merger fraction data has been binned to lower the noise; the average number has not. Once again the dashed line denotes Gaussian filtering. The solid line denotes top hat filtering, and the dotted line denotes sharp k -space filtering.

$M \ll M_*$, most of the mass selected by the filtering scheme actually resides in the halos of much more massive clusters where it may have been accreted by the larger cluster or possibly prevented from collapsing by the tidal field. Gasdynamical and other astrophysical processes could also play a strong role in modifying the faint mass end. Therefore one has little reason to believe that the low-mass slope that we determine is of relevance for the mass function of galaxies and other low-mass objects, and it should not be taken seriously beyond the regime in which it has been verified by N -body simulations. However, any of the formulae given here for the mass function can be used to provide a reasonable estimate of the high-mass end of the distribution. For the high-mass end, however, our calibrated formulae can really only be applied to estimates of the mass function of dark matter halos, which may be group and cluster halos rather than individual galaxy halos. Only with extra physical assumptions about the complex dissipative processes occurring in galaxy formation can our results be applied to galaxies rather than halos.

We close with a concrete example of the utility of the expressions we have derived, for an adiabatic cold dark matter cosmology. In Figure 16, the mass function at redshifts 1 and 3 for objects constrained to now reside in rich clusters are compared with the mass functions at those redshifts for unconstrained field objects: rare massive structures form from rare massive substructures.

We would like to thank John Peacock for many stimulating discussions on the Press-Schechter formulation. We thank Richard Epstein for drawing our attention to his 1983 solution to the cloud-in-cloud problem for Poisson fluctuations. J. R. B. and N. K. were supported in part by NSERC. J. R. B. was also supported in part by NSF under grant PHY82-17853, supplemented by funds from NASA, at the Institute for Theoretical Physics, Santa Barbara. S. C. acknowledges the support of NSF grant AST-8819802 and the CfPA at Berkeley and the hospitality of CITA. J. R. B. and N. K. are Fellows of the Canadian Institute for Advanced Research.

APPENDIX

FULL STATISTICS OF FIRST UPCROSSING POINTS

One obtains the probability $P_{\text{no up}}(\Lambda)$ that there are no upcrossing points in the resolution interval $[0, \Lambda]$ by evaluating $\langle \delta_{N_{\text{up}}(\Lambda), 0} \rangle$ where $\delta_{N, M}$ denotes the Kronecker delta (1 if $N = M$, 0 otherwise). The generating function for the moments of $N_{\text{up}}(\Lambda)$ is

$$\exp \{F_{N_{\text{up}}}(\psi)\} = \langle \exp [\psi N_{\text{up}}] \rangle = \sum_{M=0}^{\infty} e^{M\psi} P_M([0, \Lambda]), \quad P_M([0, \Lambda]) = \langle \delta_{N_{\text{up}}(\Lambda), M} \rangle.$$

The probability that the interval is a void, $P_0 = P_{\text{no up}}(\Lambda)$, is the limit of $\exp \{F_{N_{\text{up}}}(\psi)\}$ as $\psi \rightarrow -\infty$. The probability that there are exactly M upcrossing points in the interval is $P_M([0, \Lambda])$, obtained from the limit of $e^{-M\psi} \partial^M \exp [F_{N_{\text{up}}}]/\partial\psi^M$ as ψ goes to $-\infty$.

Recall that the M th moment is given by $\langle N_{\text{up}}^M \rangle = \partial^M \exp [F_{N_{\text{up}}}]/\partial\psi^M$ evaluated at $\psi = 0$, while the connected moments (cumulants) are given by $\langle N_{\text{up}}^M \rangle_c = \partial^M F_{N_{\text{up}}}/\partial\psi^M$ evaluated at $\psi = 0$. We can take out the Poisson self-correlations (the $\langle N_{\text{up}} \rangle_c$ part of $\langle N_{\text{up}}^M \rangle_c$ which appears for each M) and express this in terms of only the continuous connected correlations $\langle N_{\text{up}}^M \rangle_{cc}$ by

$$F_{N_{\text{up}}}(\psi) = \sum_{M=1}^{\infty} \frac{1}{M!} (e^\psi - 1)^M \langle N_{\text{up}}^M \rangle_{cc},$$

$$\langle N_{\text{up}}^M \rangle_{cc} = \int_0^\Lambda d\Lambda_1 \langle R_{\text{up}}(\Lambda_1) \rangle \cdots \int_0^\Lambda d\Lambda_M \langle R_{\text{up}}(\Lambda_M) \rangle \zeta^{(M)}(\Lambda_1, \dots, \Lambda_M),$$

where $\zeta^{(M)}(\Lambda_1, \dots, \Lambda_M)$ is the normalized reduced continuous M -point function. Unlike the situation with homogeneous random fields, however, the average densities $\langle R_{\text{up}}(\Lambda) \rangle$ depend upon resolution. Note that the generating function is related to the partition functional for the point process R_{up} ,

$$\exp \{\mathcal{F}_{R_{\text{up}}}[\Psi]\} \equiv \left\langle \exp \left\{ \int_0^{\Lambda_{\text{max}}} \Psi(\Lambda) R_{\text{up}}(\Lambda) d\Lambda \right\} \right\rangle,$$

$$\mathcal{F}_{R_{\text{up}}}[\Psi] = \int_0^{\Lambda_{\text{max}}} d\Lambda_1 [e^{\Psi(\Lambda_1)} - 1] \langle R_{\text{up}}(\Lambda_1) \rangle \cdots \int_0^{\Lambda_{\text{max}}} d\Lambda_M [e^{\Psi(\Lambda_M)} - 1] \langle R_{\text{up}}(\Lambda_M) \rangle \zeta^{(M)}(\Lambda_1, \dots, \Lambda_M),$$

by $F_{N_{\text{up}}}(\psi) = \mathcal{F}_{R_{\text{up}}}[\psi \chi_{[0, \Lambda]}]$.

The void probability is obtained by taking the limit, giving the expression equation (3.21). We shall now use equation (3.21) to obtain an explicit expression for the rate $\langle R_{1\text{up}} \rangle \delta\Lambda$, the probability that there is exactly one upcrossing point in the interval $[\Lambda - \delta\Lambda, \Lambda]$, and none in $[0, \Lambda - \delta\Lambda]$. To do this we must evaluate $\langle \delta_{N_{\text{up}}([0, \Lambda - \delta\Lambda, \Lambda])} \delta_{N_{\text{up}}([0, \Lambda - \delta\Lambda])} \rangle$. Using the same trick as we used for the void probability, this can be expressed as before:

$$\langle R_{1\text{up}}(\Lambda) \rangle \delta\Lambda = \lim_{\psi_1, \psi_2 \rightarrow -\infty} e^{-\psi_1} \frac{\partial}{\partial\psi_1} \langle \exp \{\psi_1 N_{\text{up}}([\Lambda - \delta\Lambda, \Lambda]) + \psi_2 N_{\text{up}}([0, \Lambda - \delta\Lambda])\} \rangle.$$

Thus we need to evaluate

$$\exp \{\mathcal{F}_{R_{\text{up}}}[\Psi]\}, \quad \text{for} \quad \Psi(\lambda_1) = \psi_1 \chi_{[\Lambda - \delta\Lambda, \Lambda]}(\lambda_1) + \psi_2 \chi_{[0, \Lambda - \delta\Lambda]}(\lambda_1).$$

We are aided by the mutual orthogonality of the characteristic functions for the two intervals, so $e^\Psi - 1 = (e^{\psi_1} - 1)\chi_{[\Lambda - \delta\Lambda, \Lambda]} +$

$(e^{\psi_2} - 1)\chi_{[0, \Lambda - \delta\Lambda]}$. Using $\chi_{[0, \Lambda - \delta\Lambda]} = \chi_{[0, \Lambda]} - \chi_{[\Lambda - \delta\Lambda, \Lambda]}$, keeping terms to order $\delta\Lambda$, and taking the $\psi_2 \rightarrow -\infty$ limit, we have

$$\mathcal{F}_{R_{\text{up}}} \rightarrow \sum_{M=1}^{\infty} \frac{(-1)^M}{M!} \langle N_{\text{up}}^M([0, \Lambda]) \rangle_{\text{cc}} + \sum_{M=1}^{\infty} \frac{(-1)^{M-1}}{(M-1)!} e^{\psi_1} \langle N_{\text{up}}([\Lambda - \delta\Lambda, \Lambda]) N_{\text{up}}^{M-1}([0, \Lambda]) \rangle_{\text{cc}} .$$

Taking the derivative with respect to e^{ψ_1} , then taking the limit finally gives equation (3.22). Using this formalism, it is easy to verify the conditional probability relations

$$\begin{aligned} \text{Probability (none in } [0, \Lambda] \mid \text{none in } [0, \Lambda - \delta\Lambda]) &= \frac{P_{\text{no up}}(\Lambda)}{P_{\text{no up}}(\Lambda - \delta\Lambda)} \\ &= 1 + \delta\Lambda \frac{\partial}{\partial \Lambda} \ln P_{\text{no up}}(\Lambda) , \end{aligned} \quad (\text{A1a})$$

$$\text{Probability (some in } [0, \Lambda] \mid \text{none in } [0, \Lambda - \delta\Lambda]) = -\delta\Lambda \frac{\partial}{\partial \Lambda} \ln P_{\text{no up}}(\Lambda) , \quad (\text{A1b})$$

$$\langle R_{1\text{up}} \rangle \approx \text{Probability (some in } [0, \Lambda] \mid \text{none in } [0, \Lambda - \delta\Lambda]) \text{ Probability (none in } [0, \Lambda - \delta\Lambda]) . \quad (\text{A1c})$$

If $\delta\Lambda$ is made small enough, “some” is one; hence equation (A1c) holds, giving the derivative relation (3.22).

Of course to evaluate the general expression, we need to know all of the reduced M -point functions of N_{up} . The *unreduced* M -point function can be evaluated:

$$\begin{aligned} 1 + \xi^{(M)}(\Lambda_1, \dots, \Lambda_M) &\equiv \frac{\langle \prod_{j=1}^M R_{\text{up}}(\Lambda_j) \rangle}{\langle \prod_{j=1}^M R_{\text{up}}(\Lambda_j) \rangle} \\ &= \frac{P_F^{(M)}(f_v, \dots, f_v) \langle \prod_{j=1}^M \dot{F}_j \mathcal{H}(\dot{F}_j) \mid F_i = f_v \rangle}{\langle \dot{F} \mathcal{H}(\dot{F}) \mid F = f_v \rangle^M} . \end{aligned} \quad (\text{A2})$$

The first term describes a positive biasing (see BBKS, Appendix F). However, the second term will add a repulsive contribution since downs must separate all ups. We have made some progress in evaluating the two-point function, but using equation (A2) to evaluate all higher *reduced* M -point functions is quite difficult. However, even if we are content with approximations to the correlations, it is well known that if we go beyond the two-point correlation level, an infinite number of higher correlations must be included.

The simplest approximation is to assume that there are no continuous correlations among the points, only Poisson (self-) correlations. Crude arguments can be given for the form of this. Then we need only include the average of N_{up} :

$$\langle R_{1\text{up}}(\Lambda) \rangle_{\text{no corr}} = \langle R_{\text{up}}(\Lambda) \rangle_{\text{up}} e^{-\langle N_{\text{up}}(\Lambda) \rangle} . \quad (\text{A3})$$

For some cases, this turns out to provide a better fit than the Peacock & Heavens (1990) formula. For example, it is essentially an exact description for the $n = -2$ power-law results and is fairly close to the CDM case. We have not found a useful approximation using the two-point function as well as the one-point function, although a consideration of its effects helps to illustrate the important physics in the problem. The continuous correlation function of the upcrossing points starts at -1 and rises to a positive peak at about the filter scale, before it drops asymptotically. This exclusion of other upcrossing points from the neighborhood of one is an important aspect to their statistics. Unfortunately, all of the N -point functions seem to be essential to give a quantitatively adequate description. In effect this is what the Peacock & Heavens formula approximates.

REFERENCES

- Babul, A. 1990, ApJ, 349, 429
- Bardeen, J. M., Bond, J. R., Kaiser, N., & Szalay, A. S. 1986, ApJ, 304, 15 (BBKS)
- Bond, J. R. 1987, in Cosmology and Particle Physics, ed. I. Hinchcliffe (Singapore: World Scientific), 22
- . 1988a, in the Early Universe, ed. W. G. Unruh (Dordrecht: Reidel), 283
- . 1988b, in Proc. Vatican Workshop on Large Scale Streaming Motions, ed. V. C. Rubin & G. V. Coyne (Princeton: Princeton University Press), 419
- . 1989, in Frontiers of Physics—From Colliders to Cosmology, ed. B. Campbell & F. Khanna (Singapore: World Scientific), 182
- Bond, J. R., Szalay, A. S., & Silk, J. 1988, ApJ, 324, 627
- Carlberg, R. G., & Couchman, H. M. P. 1989, ApJ, 340, 47
- Chandrasekhar, S. 1943, Rev. Mod. Phys., 15, 2; reprinted in Selected Papers on Noise and Stochastic Processes, ed. N. Wax (New York: Dover 1954)
- Cole, S. 1991, ApJ, 367, 45
- Cole, S., & Kaiser, N. 1988, MNRAS, 233, 637
- . 1989, MNRAS, 237, 1127
- Davis, M., Efstathiou, G., Frenk, C., & White, S. D. M. 1985, ApJ, 292, 371
- Efstathiou, G. P., & Bond, J. R. 1986, MNRAS, 218, 103
- . 1987, MNRAS, 227, 33P
- Efstathiou, G., & Rees, M. 1988, MNRAS, 230, 5P
- Efstathiou, G., Frenk, C. S., White, S. D. M., & Davis, M. 1988, MNRAS, 235, 715
- Epstein, R. 1983, MNRAS, 205, 207
- Kaiser, N. 1988, in IAU Symposium 130, Large Scale Structures in the Universe, ed. J. Audouze, M.-C. Pelletan, & A. Szalay (Dordrecht: Reidel), 43
- Narayan, R., & White, S. D. M. 1987, MNRAS, 231, 97P
- Peacock, J. A., & Heavens, A. F. 1990, MNRAS, 243, 133
- Peebles, P. J. E. 1980, The Large-Scale Structure of the Universe (Princeton: Princeton University Press)
- . 1987, ApJ, 277, L1
- Press, W. H., & Schechter, P. 1974, ApJ, 187, 425 (PS)
- Schaeffer, R., & Silk, J. 1985, ApJ, 292, 319
- . 1988, ApJ, 332, 1
- White, S. D. M. 1979, MNRAS, 186, 145